united nations
educational, scientific
and cultural
organization

international atomic
energy agency

the
abdus salam
international centre for theoretical physics

ICTP 40th Anniversary

SCHOOL ON SYNCHROTRON RADIATION AND APPLICATIONS
In memory of J.C. Fuggle & L. Fonda

19 April - 21 May 2004

Miramare - Trieste, Italy

1561/42

Methodology of PEEM and XPEEM experiments and image processing

A. Locatelli

Methodology of PEEM and XPEEM experiments and image processing

Andrea Locatelli

Contributors

Elettra

S. Heun, M. Kiskinova

Around the world

S. Cherifi, T. Schmidt, S. Günther

XPEEM instrumentation

C. Koziol (Elmitec)

J. Westermann, B. Holmes (Omicron)

Motivations

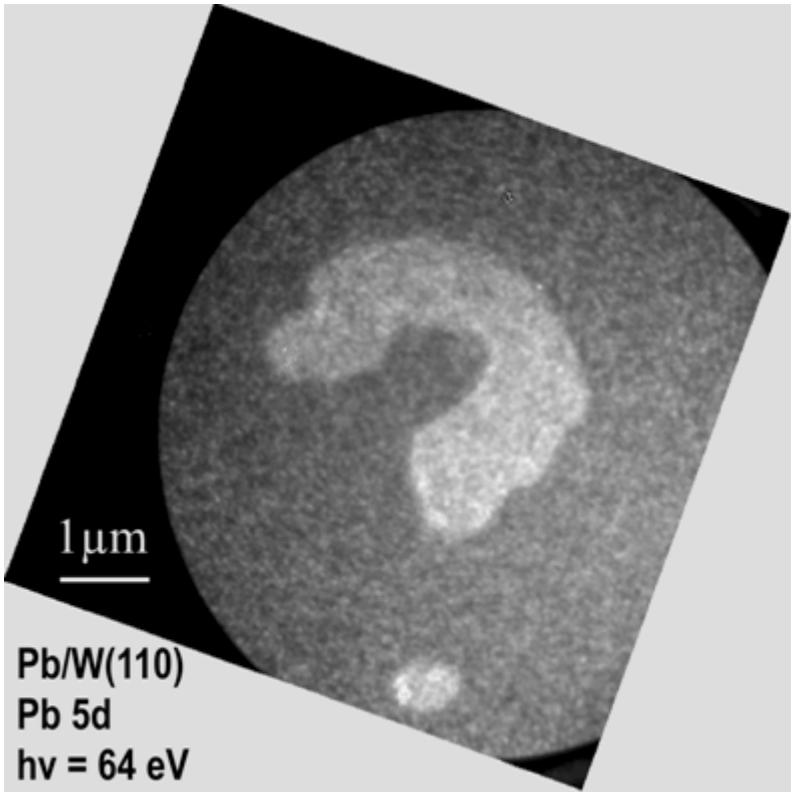

Why XPS?

- element sensitive
- chemical shift
- surface sensitive

Why spectromicroscopy ?

- nanostructures self-organization
- devices (lithography)
- diffusion, segregation
- alloying
- chemical reactions
- magnetism (XMCD)

Magnetic Studies

SR Instrumentation and experiments

Concepts - XAS

XMCD

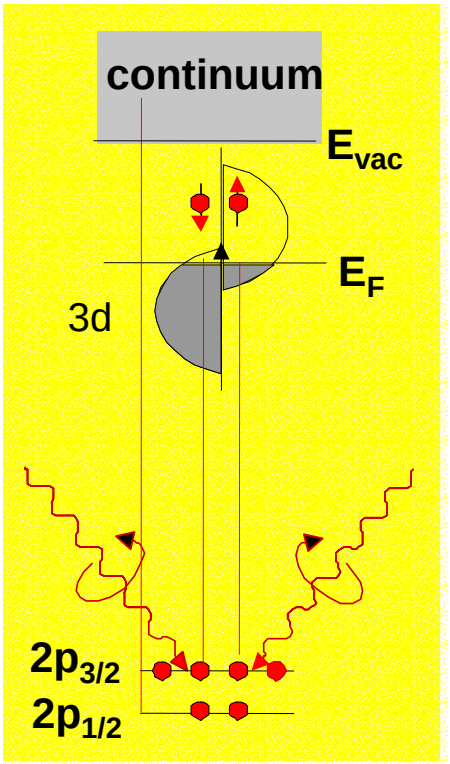

ferromagnetic

XMLD

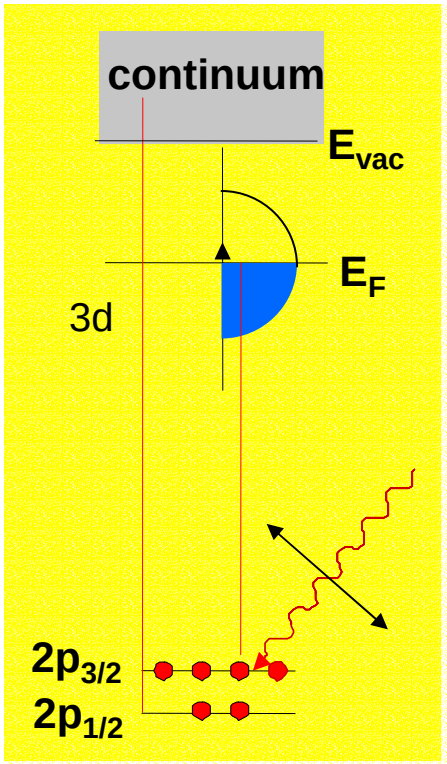

anti-ferromagnetic

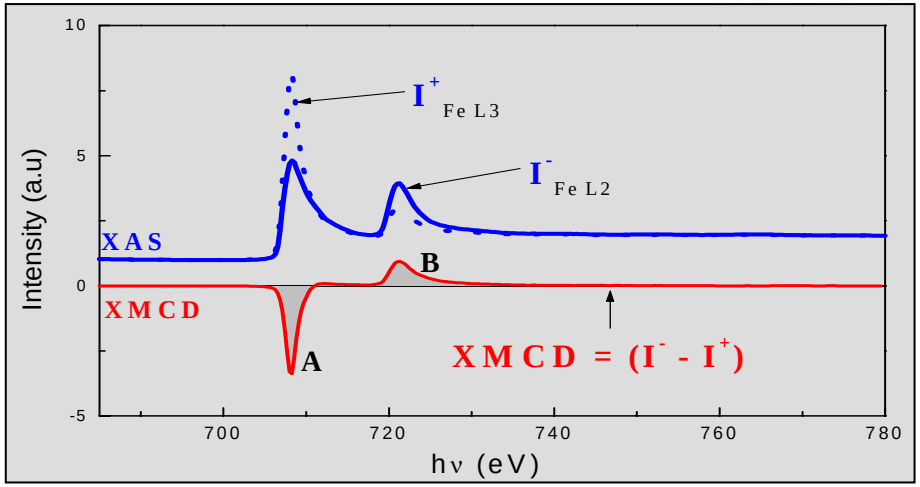

Sum Rules

Spin magnetic moment

$$[\mathbf{A} - 2\mathbf{B}] = -C/\mu_B \; M_S^{eff}(\theta,\varphi)$$

Orbital moment

$$[\mathbf{A} + \mathbf{B}] = -3C/2\mu_B \; M_L(\theta,\varphi)$$

B. T. Thole, P. Carra, F. Sette, and G. van der Laan, Phys. Rev. Lett. 68, 1943 (1992); P. Carra, B. T. Thole, M. Altarelli, and X.Wang, Phys. Rev. Lett. 70, 694 (1993), J.Stöhr et al, Phys. Rev. Lett. 75 (1995) 3748.

XMCD and XMLD

Magnetic imaging with elemental sensitivity

Direct observation of the alignment of ferromagnetic spins by antiferromagnetic spins

F. Nolting*, A. Scholl*, J. Stöhr†, J. W. Seo‡§, J. Fompeyrine§, H. Siegwart§, J.-P. Locquet§, S. Anders*, J. Lüning†, E. E. Fullerton†, M. F. Toney†, M. R. Scheinfein‖ & H. A. Padmore*

Nature, 405 (2000), 767.

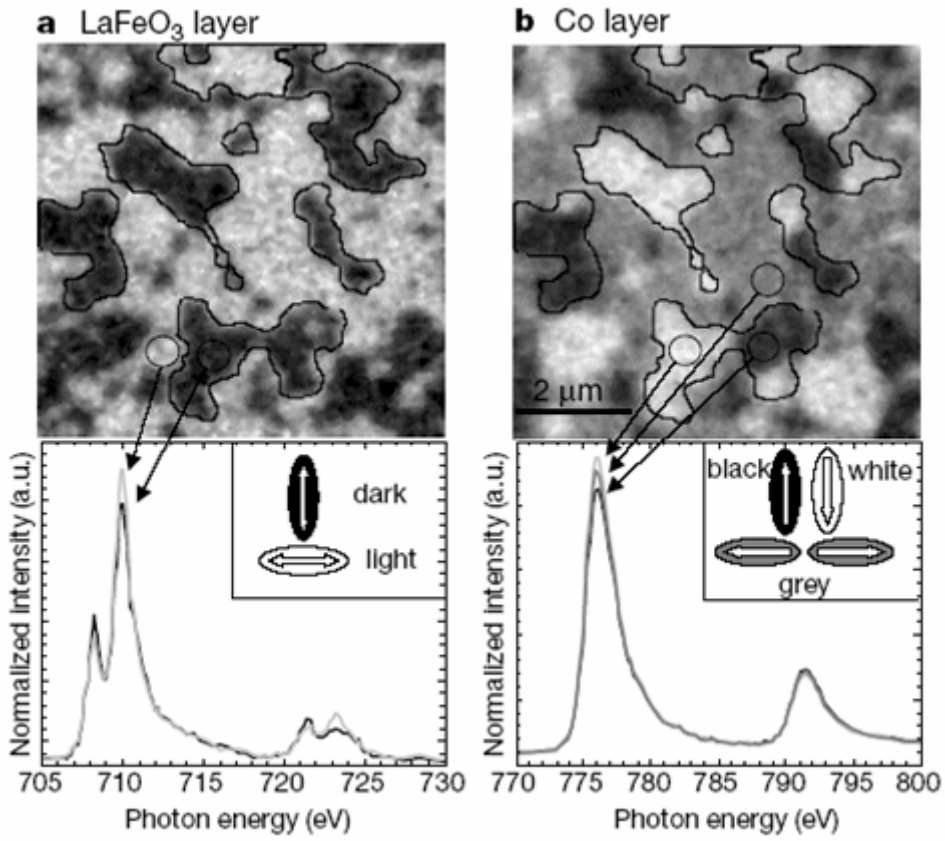

Figure 1 Images and local spectra from the antiferromagnetic and ferromagnetic layers for 1.2-nm Co on $LaFeO_3/SrTiO_3(001)$. **a**, Fe L-edge XMLD image; **b**, Co L-edge XMCD image. The contrast in the images arises from antiferromagnetic domains in $LaFeO_3$ (**a**) and ferromagnetic domains in Co (**b**) with in-plane orientations of the antiferromagnetic axis and ferromagnetic spins as indicated below the images. The spectra shown underneath were recorded in the indicated areas and illustrate the origin of the intensity contrast in the PEEM images.

Magnetic imaging at Elettra

The “Nanospectroscopy” beamline

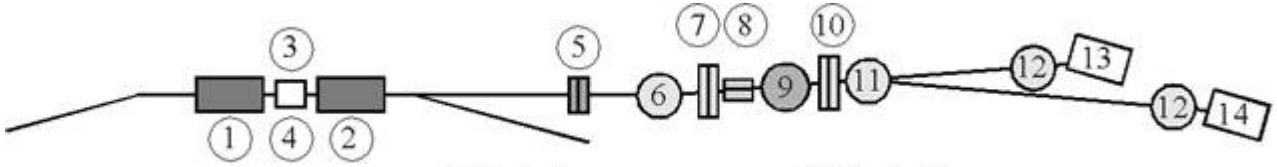

1: Section 1.1
2: Section 1.2
3: Modulator
4: Source
5: Pinhole
6: Toroidal mirror
7: Entrance Slit (horiz.)
8: Entrance Slit (vert.)
9: Monochromator
10: Exit-slit
11: Deflection mirror
12: Refocussing pair
13: SPELEEM
14: Second branch end station

Source: Variable Polarization, helical undulator

Monochromator: Wide spectral range
Medium spectral resolution

Spot: High photon flux density on sample
Small variable spot size (~µm)
Homogeneous illumination

Microscope: SPELEEM (Elmitec)

Front End

Monochromator

Refocusing Mirrors

SPELEEM

2nd Branch

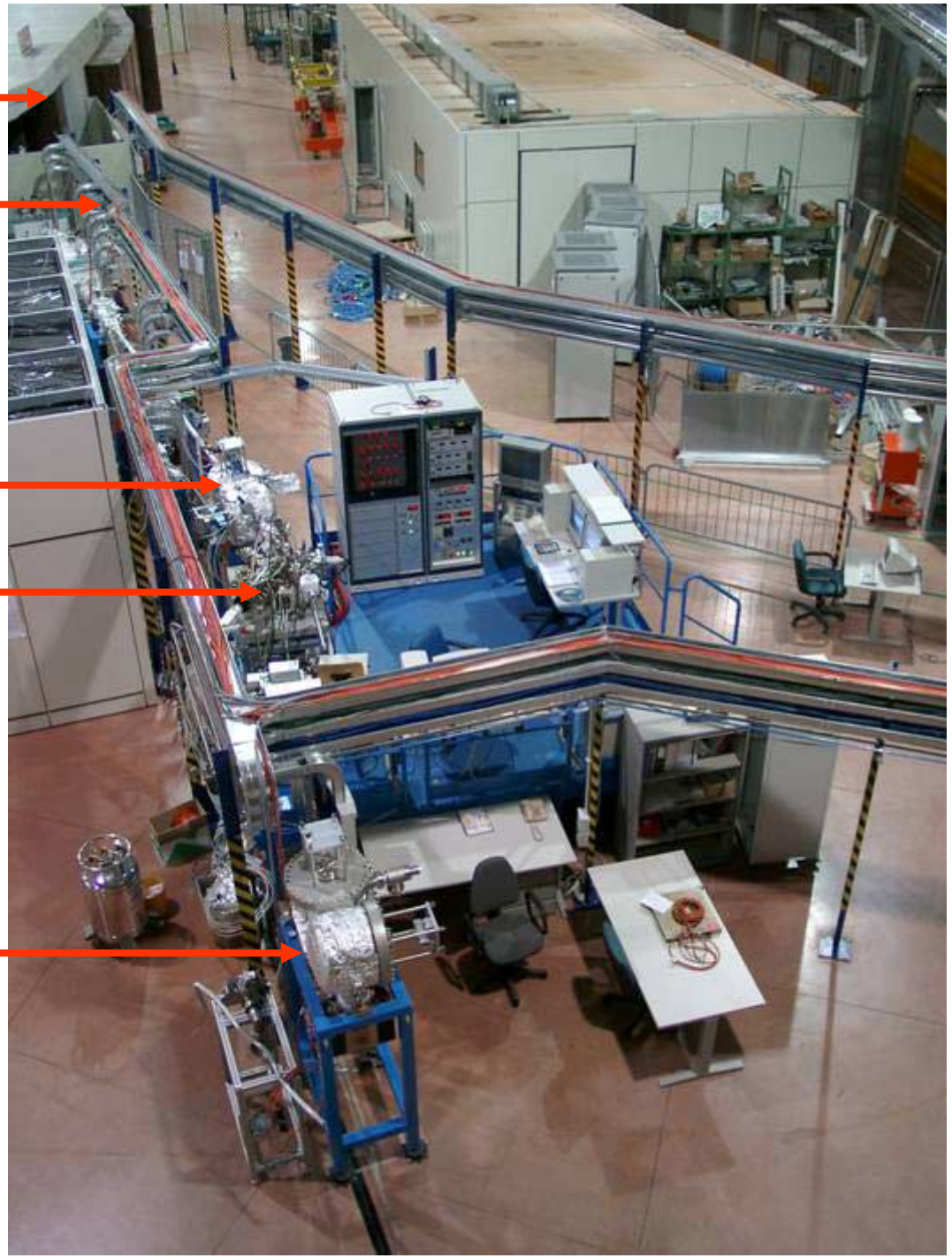

Beamline source

- FEL/Nanospectroscopy undulator
- Sasaki Apple II type undulator

- 2 sections with phase modulation electromagnet
- 2 x 20 periods of length 10 cm

- Polarization: elliptical (horizontal, circular, and vertical)

- Source dimension: 560 μm x 70 μm

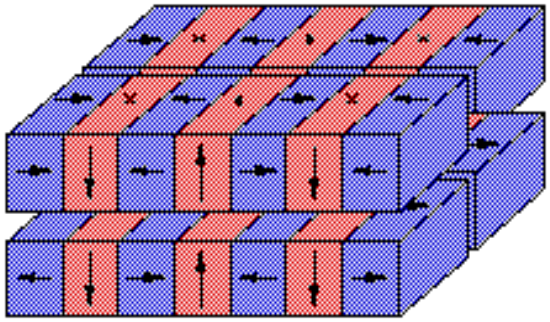

Undulator characteristics

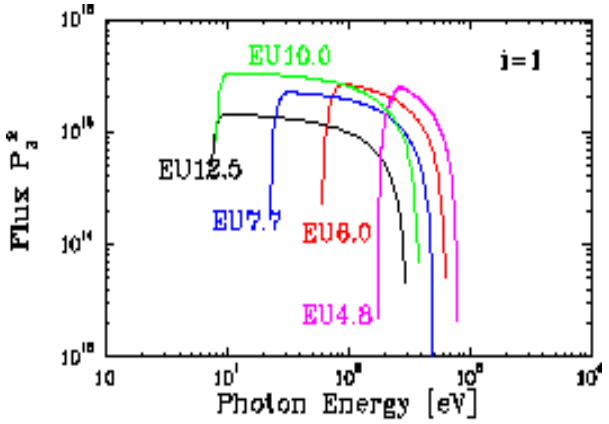

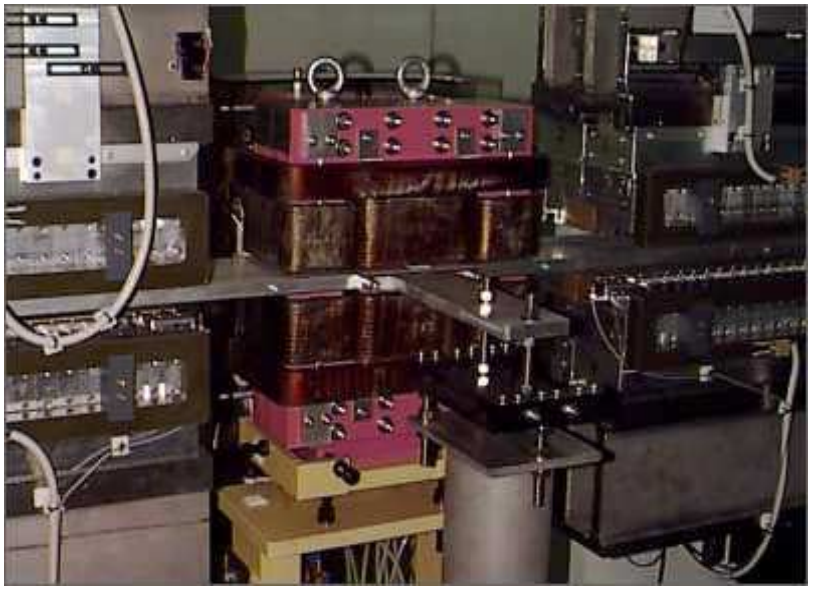

Monochromator

- 2 VLS (variable line spacing) gratings of low groove density
  - 200/mm for 20 - 250 eV
  - 400/mm for 200 - 1000 eV

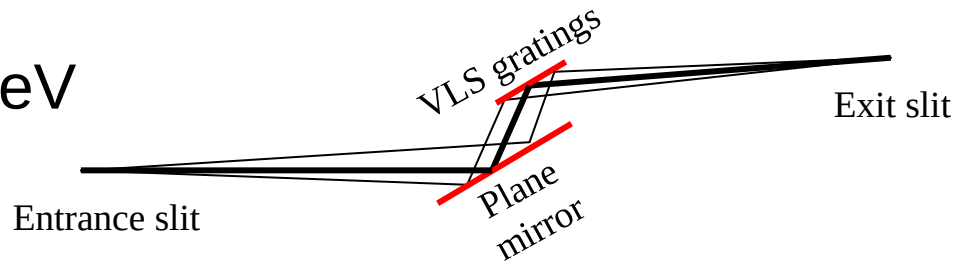

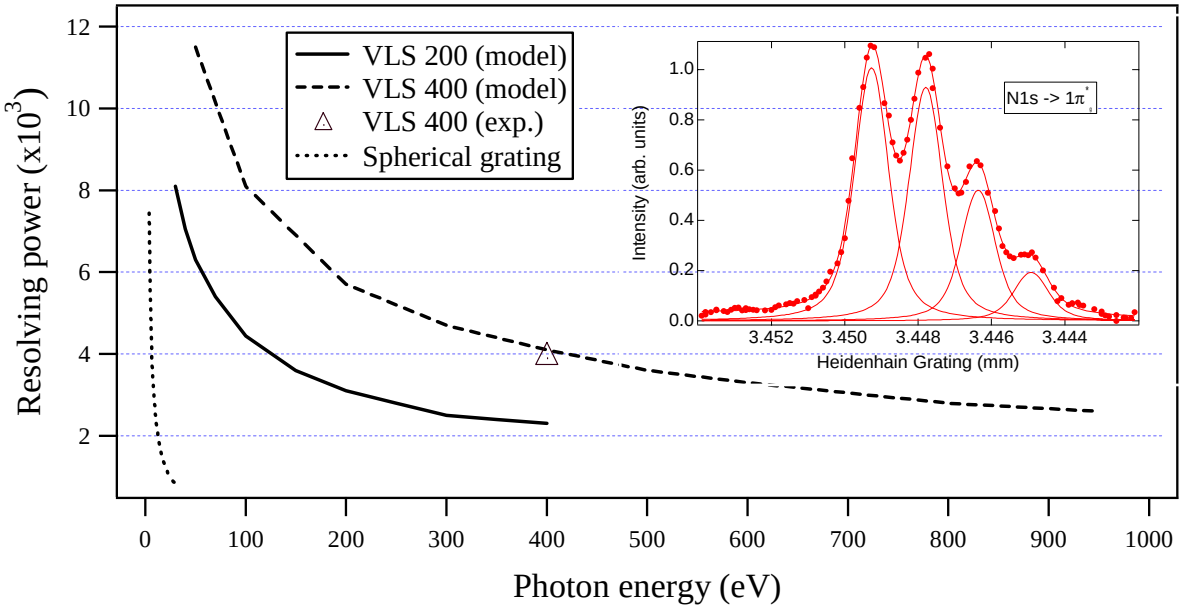

Photon beam refocussing

- Need:
  - Homogeneous micro-spot
  - Highest photon flux in the field of view of the microscope
- Two adaptive plane elliptical mirrors («bendable mirrors»)
- Bend by applying unequal moments to their ends
- Kirkpatrick-Baez configuration
- Theoretical spot size:

  1.6 µm (vert) x 6.1 µm (hor)

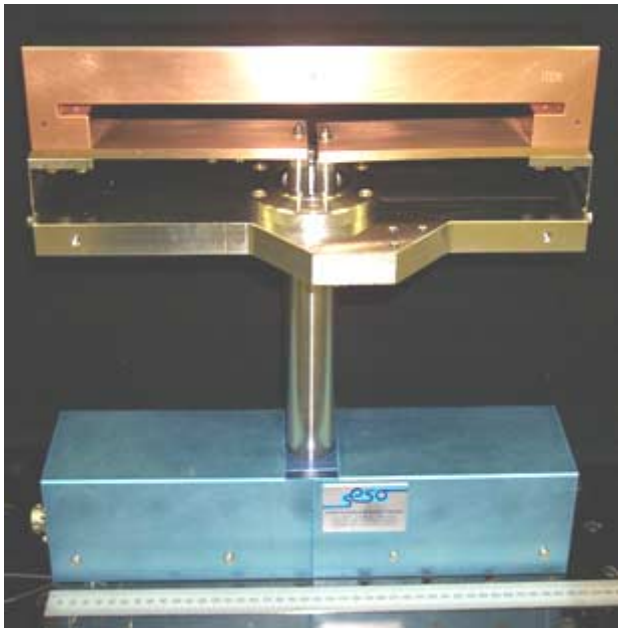

A. Bianco, G. Sostero, and D. Cocco: Proc. SPIE 4782 (2002) 74.

Spot size

Best Focus

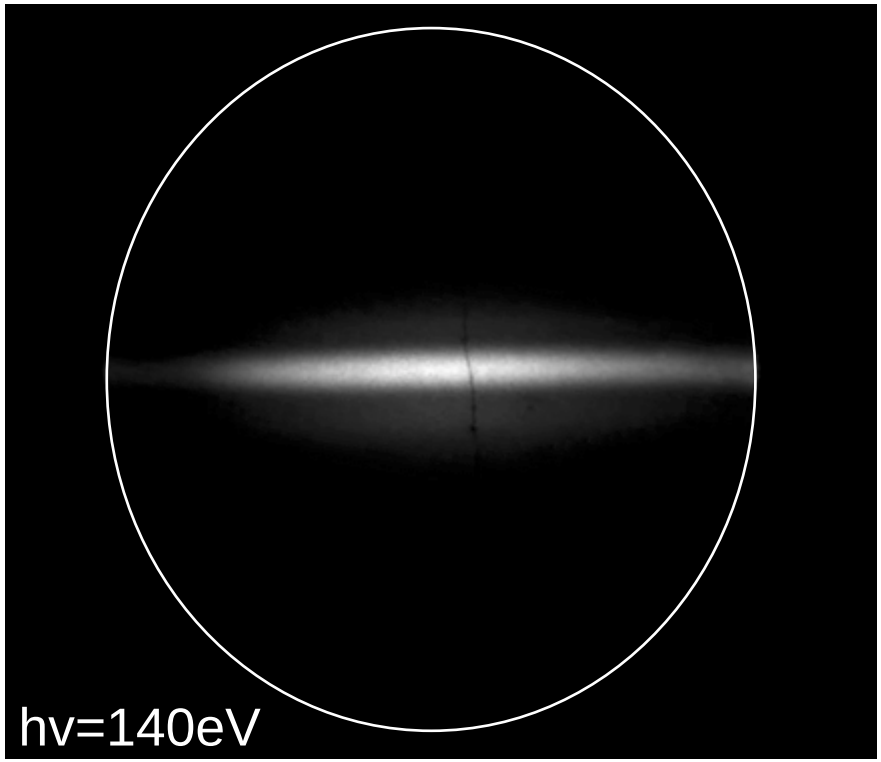

Field of view: 55 µm

vertical line profile (FWHM 2 µm)

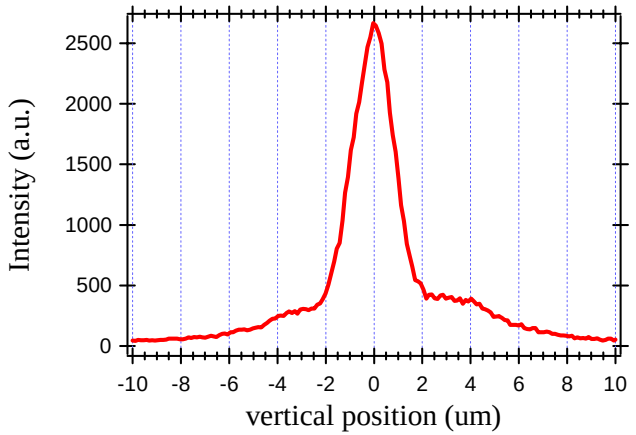

horizontal line profile (FWHM 25 µm)
corrected for grazing incidence: 7 µm

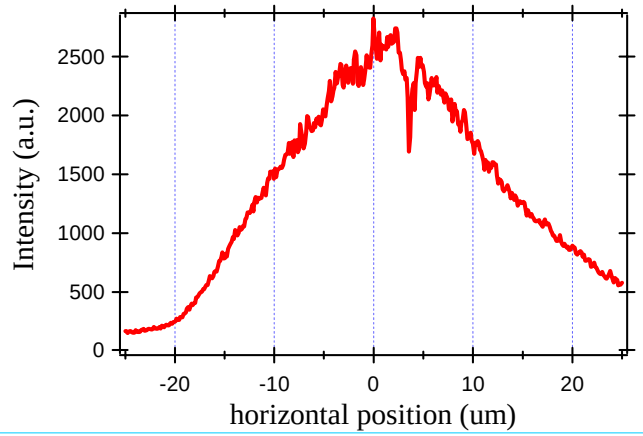

A. Bianco, G. Sostero, and D. Cocco: Proc. SPIE 4782 (2002) 74.

Beamline photon flux

Phase = 0 mm (linear pol.)

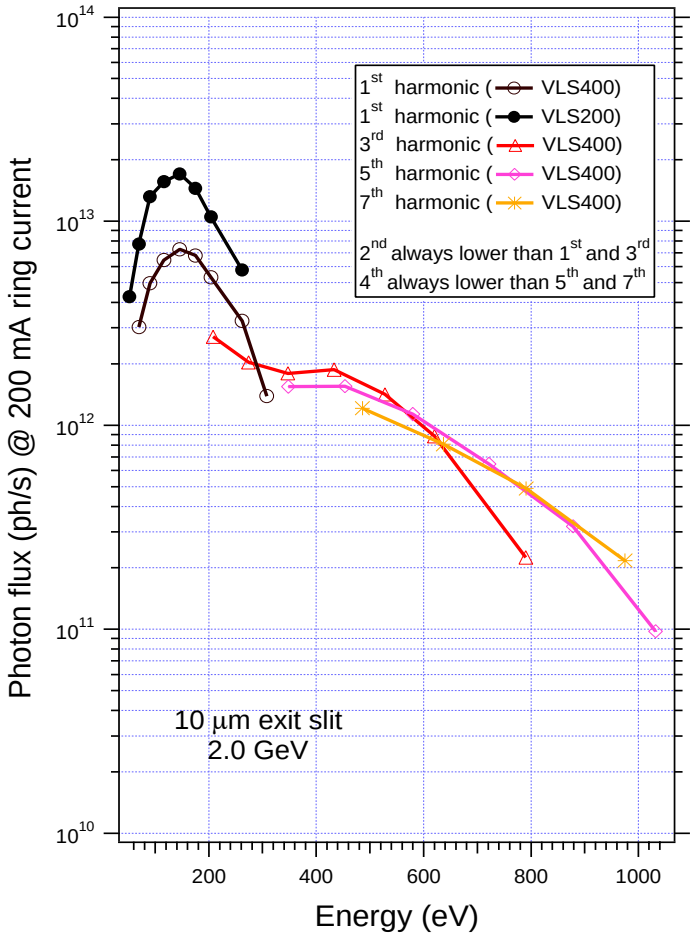

Phase = 35 mm (circ. pol.)

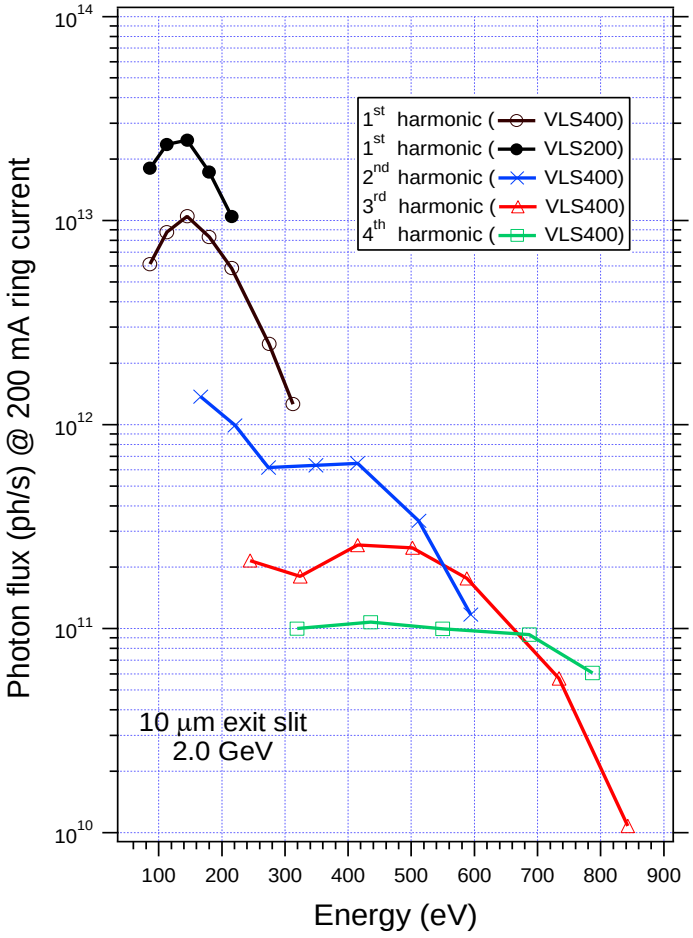

A. Locatelli, A. Bianco, D. Cocco, S. Cherifi, S. Heun, M. Marsi, M. Pasqualetto, and E. Bauer: J. Phys. IV **104** (2003) 99.

High lateral resolution

Domain structure

of 1.6 μm wide Co rings

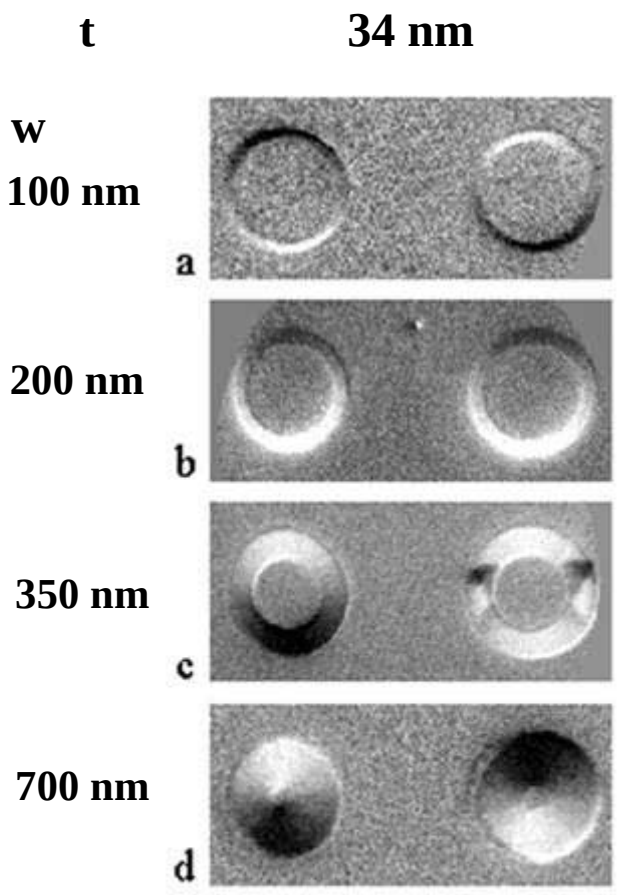

Helicity fast switching

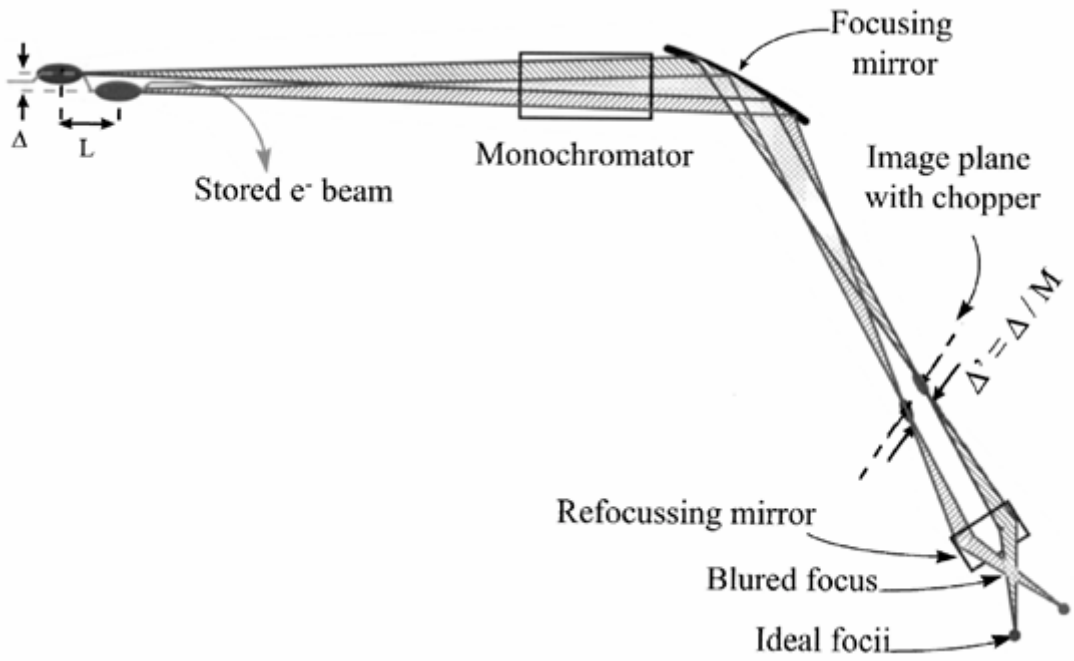

ELSEVIER
Surface Science 480 (2001) 173–179
SURFACE SCIENCE
www.elsevier.nl/locate/susc

A beamline for time resolved photoelectron microscopy on magnetic materials at the Swiss light source

C. Quitmann [a,*], U. Flechsig [a], L. Patthey [a], T. Schmidt [a], G. Ingold [a], M. Howells [b], M. Janousch [a], R. Abela [a]

[a] Paul Scherrer Institut, Swiss Light Source, CH-5232 Villigen-PSI, Switzerland
[b] Advanced Light Source, Lawrence Berkeley National Laboratory, Berkeley, CA 94720, USA

Our design also uses two IDs located one behind the other, but as a novel feature the optical paths for the two photon beams overlap almost completely. Therefore it is sufficient to use a single set of relatively small mirrors to accept and guide both photon beams. The operation principle is shown in Fig. 1. Two IDs are located in the same straight section one behind the other. Each of them acts as a radiation source. Using steerer magnets located before, between, and after the IDs a small parallel offset is created in the electron orbit. This causes a separation of the two source points by L in longitudinal and by Δ in transverse direction. The IDs are set to the same photon energy, but to opposite helicity. A focusing mirror having demagnification $1/M$, located behind the monochromator images these two source points onto the image plane. Here the two sources cause two images separated by $\Delta' = \Delta/M$. A mechanical chopper, located in the image plane, alternatively blocks one of the two photon beams. This arrangement now provides a beam of photons with switchable helicity. The two photon beams can be overlapped on the sample using a single refocussing mirror. This mirror creates two images of the two source points, but in front of the ideal focus, the two photon beams overlap in a blurred focus, see Fig. 1. As long as the source separation Δ is small, this blurred focus is close to the ideal focus and its diameter is comparable to that of the ideal focus.

Beamline design

SLS “Surface/Interface microscopy”

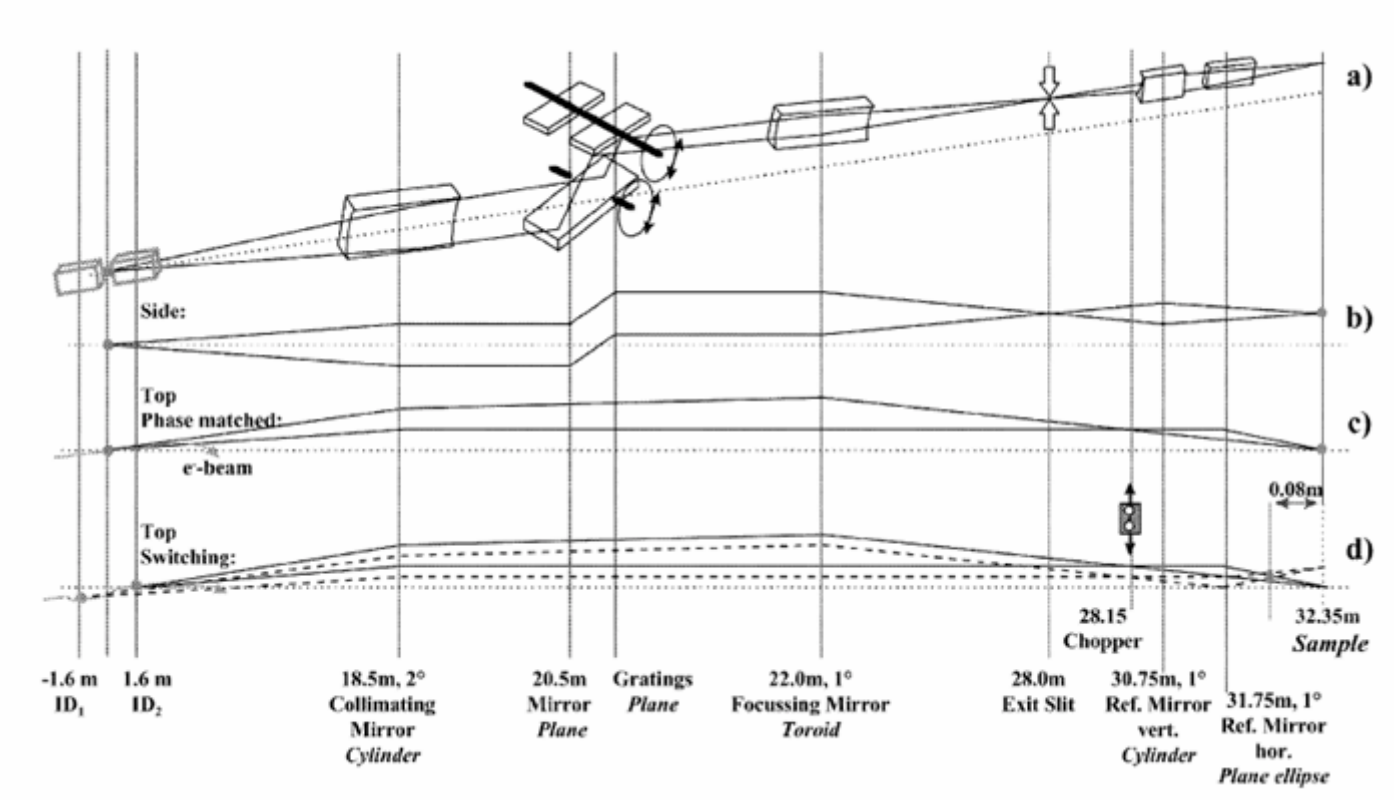

Time resolved experiments

“Pump and probe”

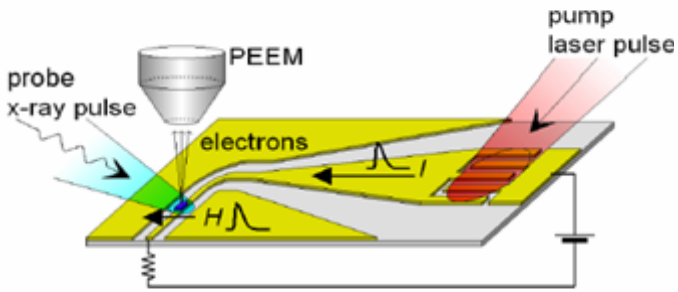

FIG. S1. Schematic of the experimental arrangement.

Experimental Setup

The experimental setup is shown in Fig. S1. Fast in-plane field pulses on top of a waveguide are derived from current pulses, launched in a photoconductive switch. The switch is activated by pulses from a Ti:Sapphire laser of 800 nm wavelength at 125 MHz repetition rate. The current pulses have a fast rising edge below the resolution of this experiment and an amplitude of about 15 mT. They decay exponentially with a time constant of about 300 ps. The sample is probed by soft x-rays from the bending magnet beamline 7.3.1.1 of the Advanced Light Source (ALS). The spot size is about 30x30 μm^2. The x-rays are pulsed at a repetition rate of 3.05 MHz, phase-locked to the laser pulses. At this frequency every 41st pump field pulse is probed. The time evolution of the state of the sample is measured by varying the electronic delay between the pump pulse and the probe pulse with an accuracy of about 20 ps. The laser frequency limits the scan range to 0-8 ns. The time resolution of the measurement is determined by the length of the x-ray pulse of about 70 ps.

Domain dynamics imaging

Science, 304 (2004), 420

Vortex Core–Driven Magnetization Dynamics

S.-B. Choe,[1]* Y. Acremann,[2] A. Scholl,[1] A. Bauer,[1,2,3] A. Doran,[1] J. Stöhr,[2] H. A. Padmore[1]

Time-resolved x-ray imaging shows that the magnetization dynamics of a micron-sized pattern containing a ferromagnetic vortex is determined by its handedness, or chirality. The out-of-plane magnetization in the nanometer-scale vortex core induces a three-dimensional handedness in the planar magnetic structure, leading to a precessional motion of the core parallel to a subnanosecond field pulse. The core velocity was an order of magnitude higher than expected from the static susceptibility. These results demonstrate that handedness, already well known to be important in biological systems, plays an important role in the dynamics of microscopic magnets.

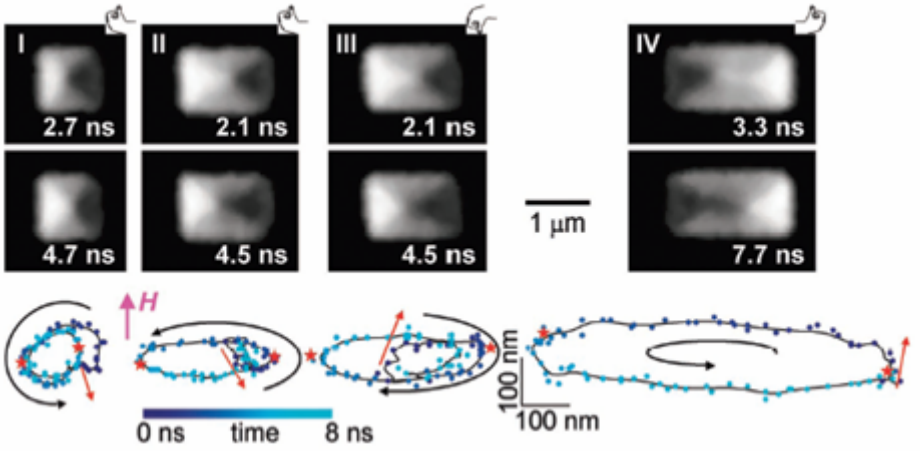

Fig. 1. (**Top**) Domain images of the in-plane magnetization of Pattern I (1 × 1 μm²), Patterns II and III (1.5 × 1 μm²), and Pattern IV (2 × 1 μm²), taken at the specified delay times after the field pulse. The images are part of a time series that extends over 8 ns and were chosen so that the horizontal displacement of the vortex has maximum amplitude. Hands illustrate the vortex handedness and the out-of-plane core magnetization as determined from the vortex dynamics. (**Bottom**) Trajectories of the vortex core. The dots represent sequential vortex positions (in 100-ps steps). Lines represent time-averaged positions with a Gaussian weight function of 100 ps (FWHM) for 0 to 1 ns and 400 ps (FWHM) for 1 to 8 ns. The progression in time is symbolized by the dot color. Red arrows show the trajectory during the field pulse; black arrows show the direction of gyrotropic rotation after the pulse; and red stars show the vortex position for the shown domain images.

Magnetisation dynamics

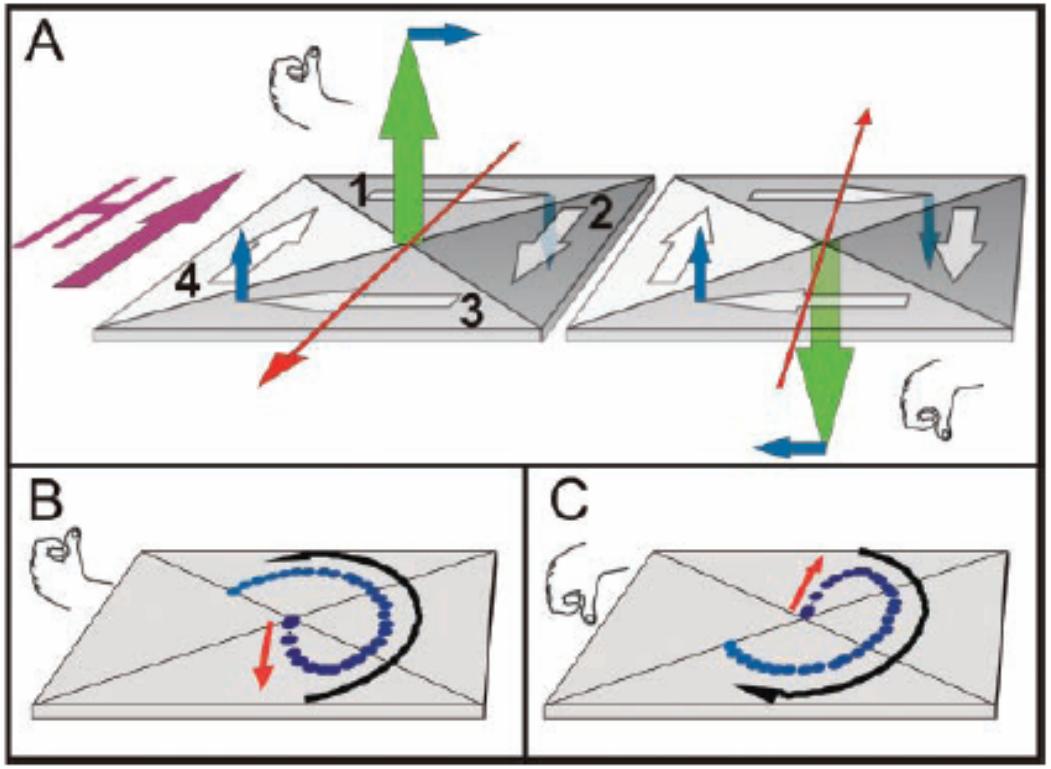

Fig. 2. (**A**) Spin structure (white arrows) of a left-handed (left side) and a right-handed (right side) square vortex. Blue arrows represent the precessional torque generated by the external magnetic field (purple arrow). Hands illustrate the vortex handedness, and a green arrow indicates the out-of-plane core magnetization. Red arrows indicate the acceleration direction in response to the field. (**B** and **C**) Simulated trajectory of the core of (B) a left-handed and (C) a right-handed vortex during and after a field pulse.

Chemical Studies

Methodology and Instrumentation

PEM concepts

XPS – mode: hν=const

hν in / e^- out

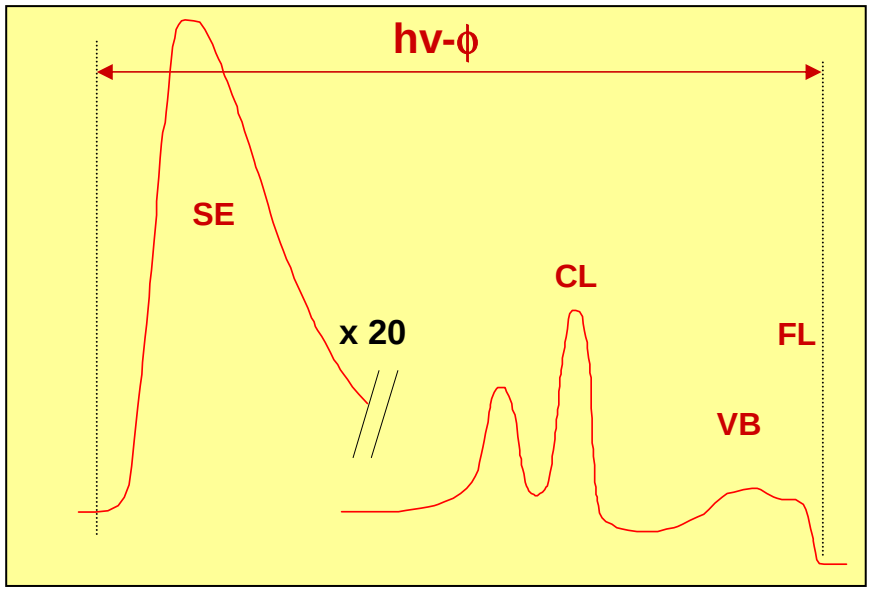

Collection modes:

Total yield mode – all emitted PE
Low/high pass filtering
Band pass filtering

Instrumental approach

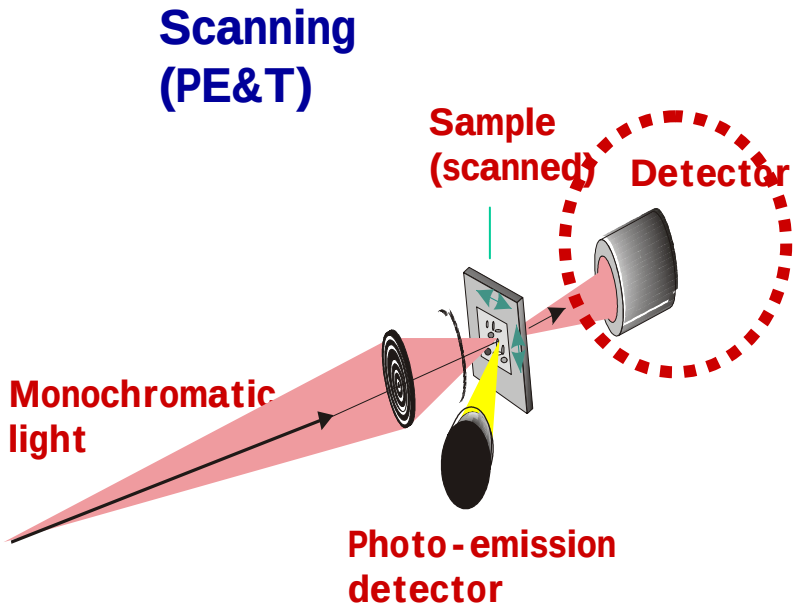

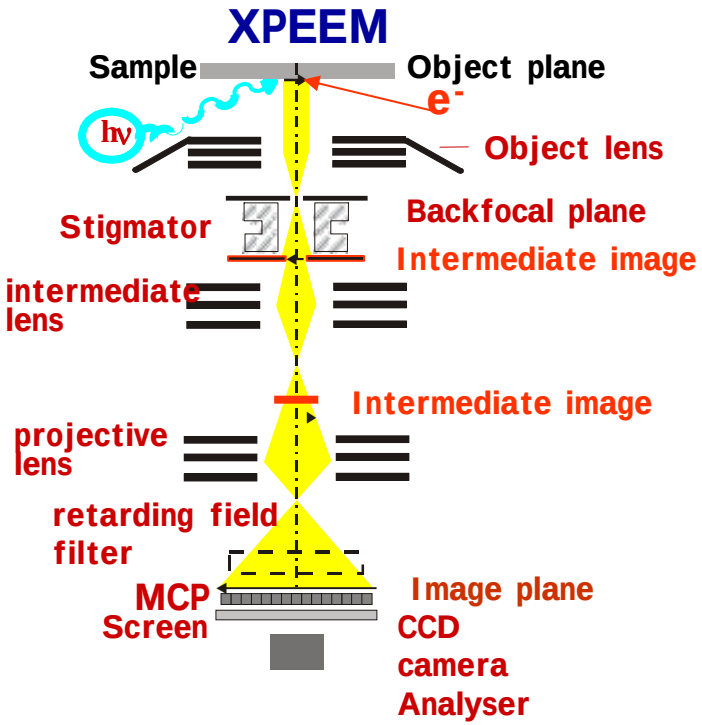

Photon optics is de-magnifying the beam:

Scanning Instrument

1. Whole power of XPS in a small spot mode.
2. Flexibility for adding different detectors.
3. Rough surfaces can be measured.
4. Limited use for fast dynamic processes.
5. Lower resolution than imaging instruments.

Electron optics to magnify irradiated area:

Imaging Instrument

1. High lateral resolution (20 nm).
2. Multi-method instrument (XPEEM/PED).
3. Excellent for monitoring dynamic processes.
4. Poorer spectroscopic ability.
5. Sensitive to rough surfaces.

Cathode lens properties

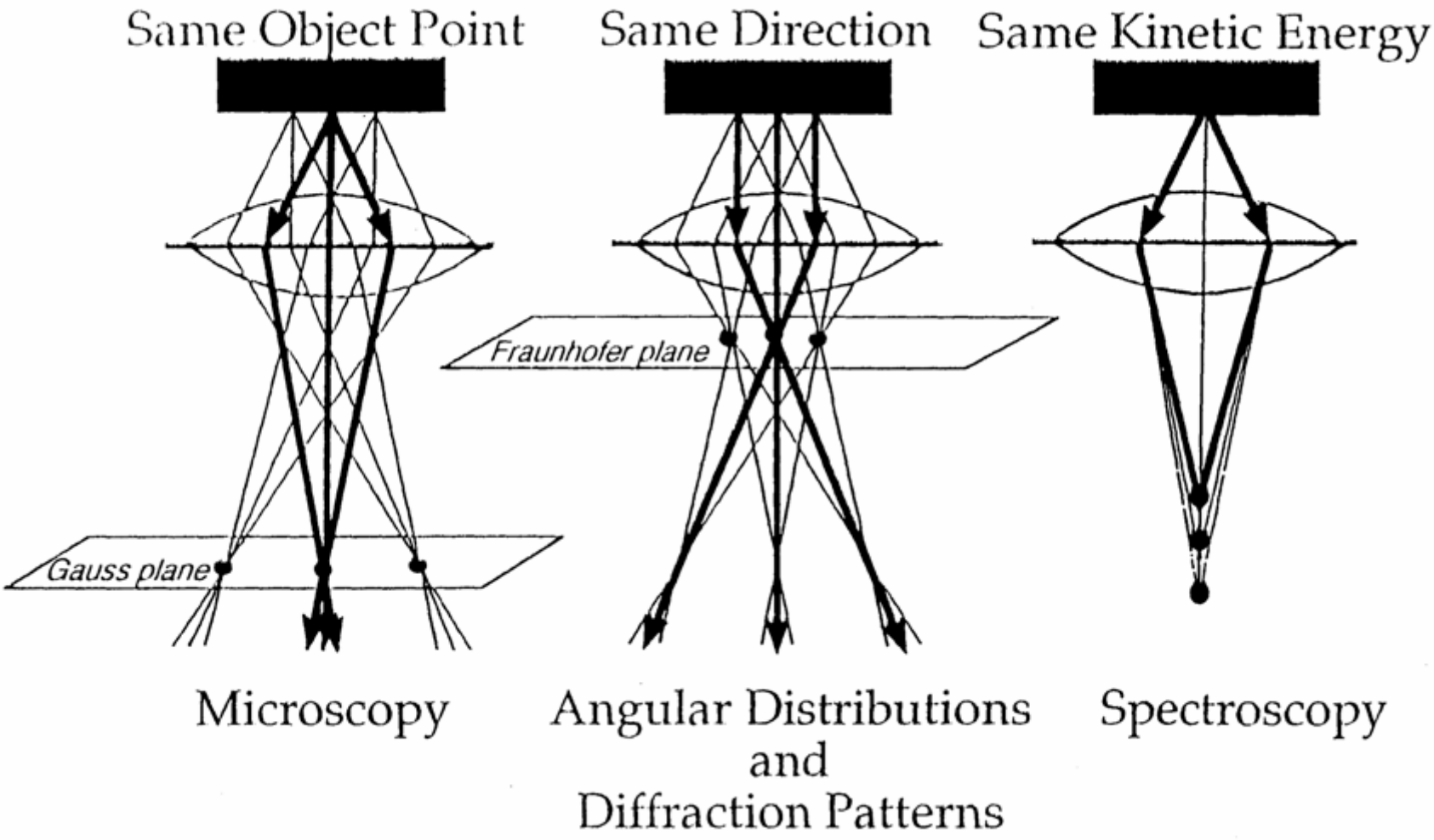

PEEM instruments

- PEEM without energy filter
- PEEM with imaging retarding field filter
- PEEM with area selective spectroscopy
- PEEM with full spectro-microscopic capabilities
- PEEM with sector field (LEEM)
- PEEM with aberration correction

PEEM without energy filter

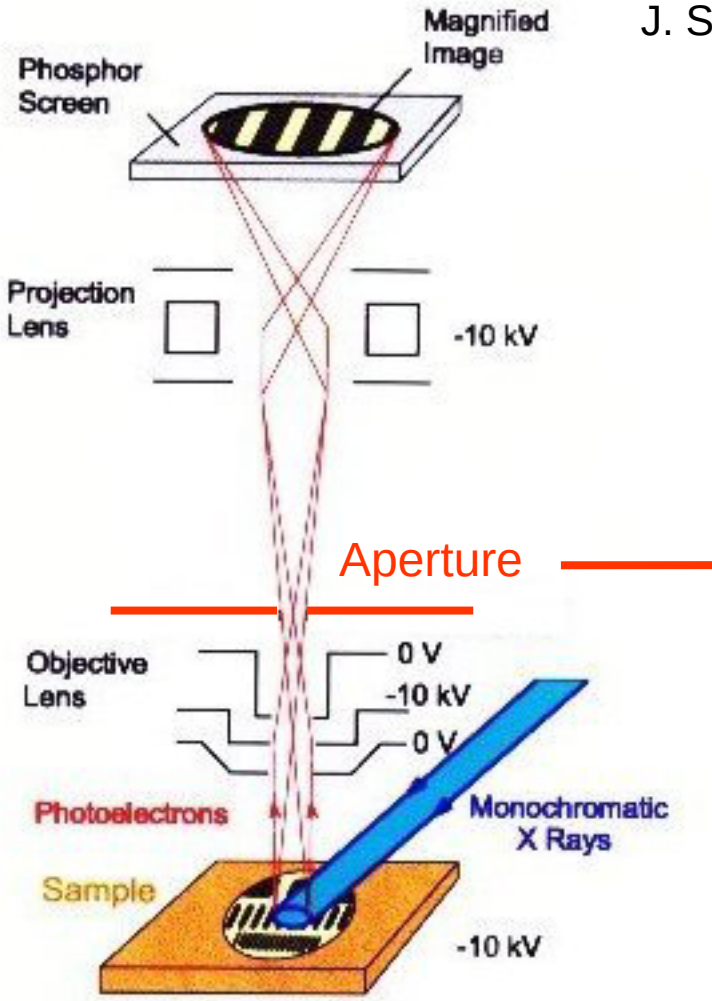

J. Stöhr et al.: Surf. Rev. Lett. **5** (1998) 1297

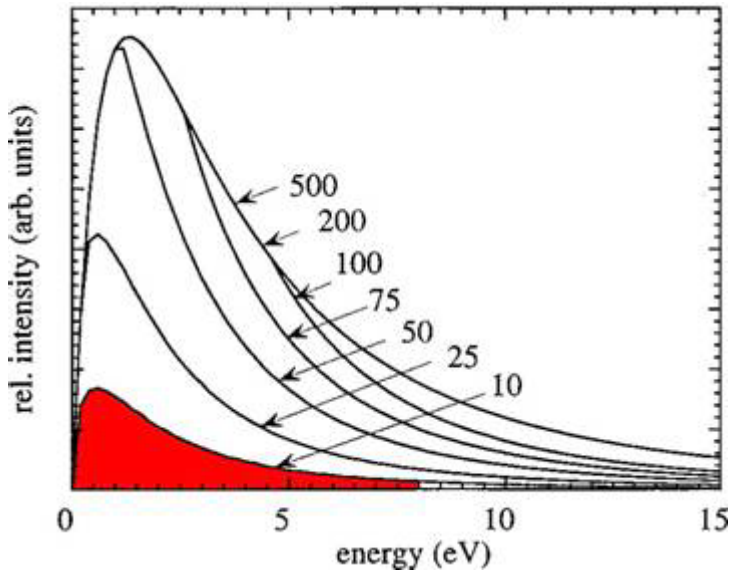

S. Anders et al.: Rev. Sci. Instrum. **70** (1999) 3973

Oscillatory reactions

PEEM - Work function contrast and Time resolved capability

VOLUME 65, NUMBER 24 PHYSICAL REVIEW LETTERS 10 DECEMBER 1990

Spatiotemporal Concentration Patterns in a Surface Reaction: Propagating and Standing Waves, Rotating Spirals, and Turbulence

S. Jakubith, H. H. Rotermund, W. Engel, A. von Oertzen, and G. Ertl
Fritz-Haber-Institut der Max-Planck-Gesellschaft, Faradayweg 4-6, D-1000 Berlin 33, Germany
(Received 25 June 1990)

Laterally varying surface concentrations associated with the oscillatory oxidation of carbon monoxide on a Pt(110) surface were imaged by photoemission electron microscopy. Depending on the applied conditions, a large variety of spatiotemporal patterns were observed that are characteristic for the nonlinear dynamics of reaction-diffusion systems.

Examples

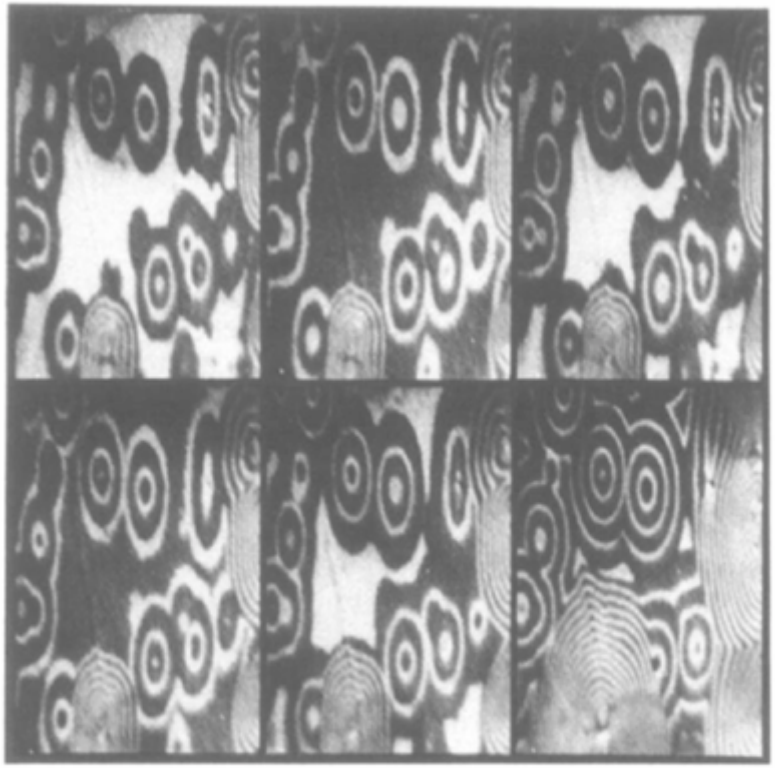

FIG. 1. Sequence of target patterns on a 0.2×0.3-mm^2 section of the Pt(110) surface at $T=427$ K, $p_{CO}=3\times10^{-5}$ mbar, and $p_{O_2}=3.2\times10^{-4}$ mbar. The time interval between the first five images is 4.1 sec; the time interval between the last two images is 30 sec.

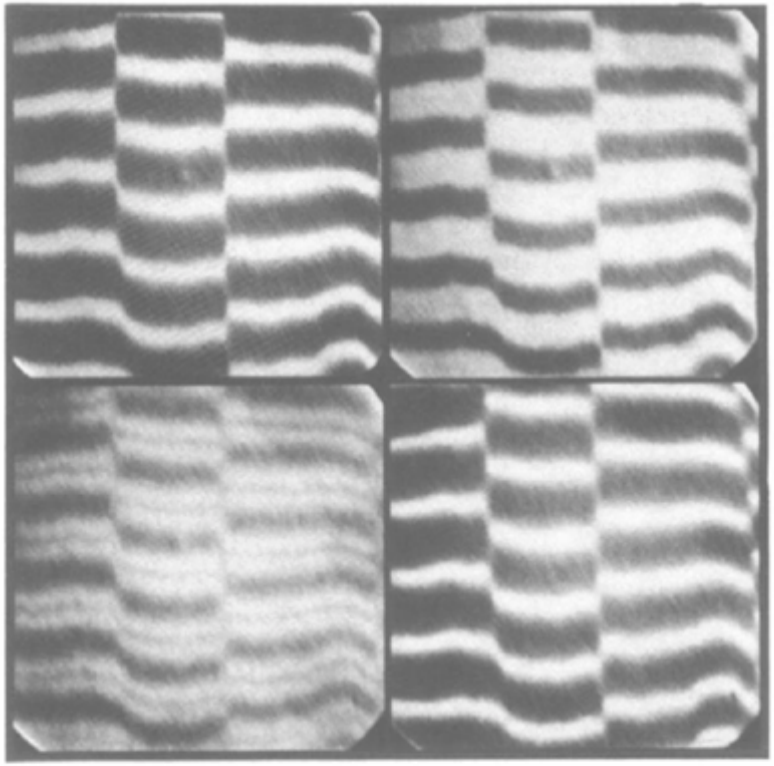

FIG. 3. Standing-wave-type patterns on a 0.3×0.3-mm^2 surface area accompanying rapid harmonic temporal oscillations with a period duration of $\tau=1.4$ sec. $T=550$ K, $p_{CO}=1.75\times10^{-4}$ mbar, and $p_{O_2}=4.1\times10^{-4}$ mbar. $t=0$, 0.08, 0.12, and 0.46 sec.

Energy filtered PEEMs

Hemispherical Analyzer

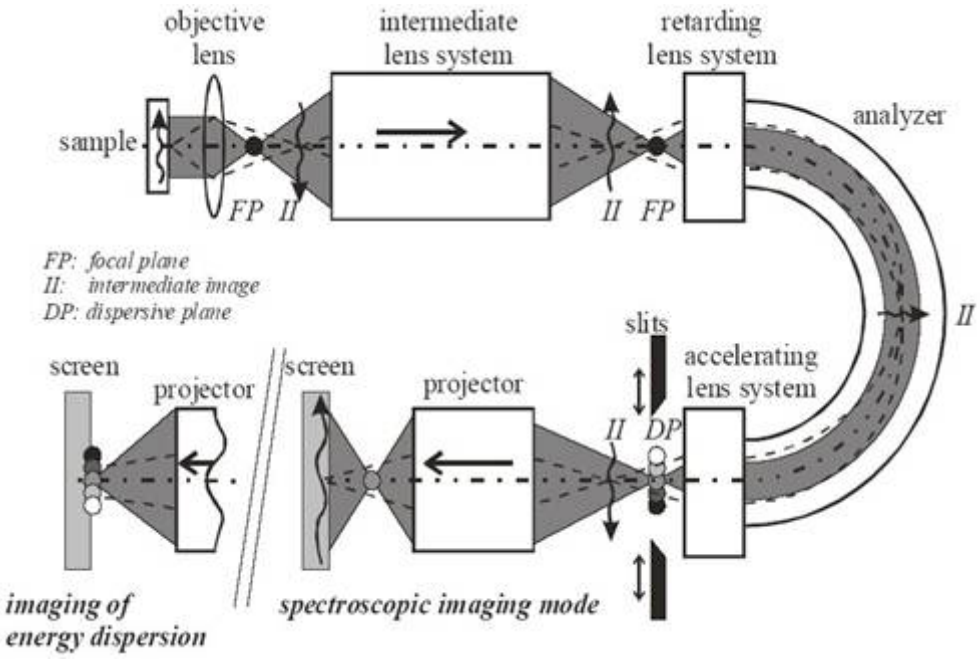

Double Hemispherical Analyzer

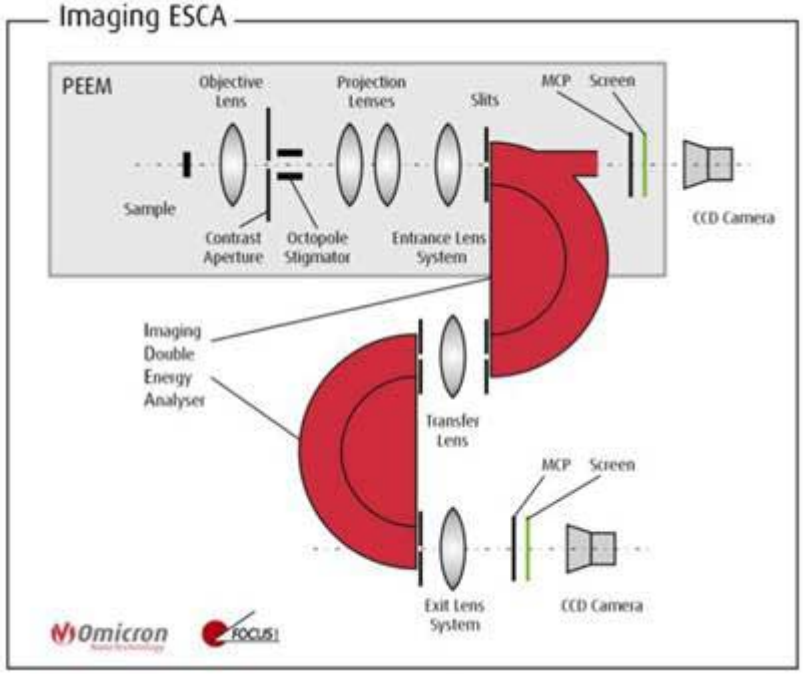

The SPELEEM microscope

Spectroscopic photoemission and low energy electron microscope

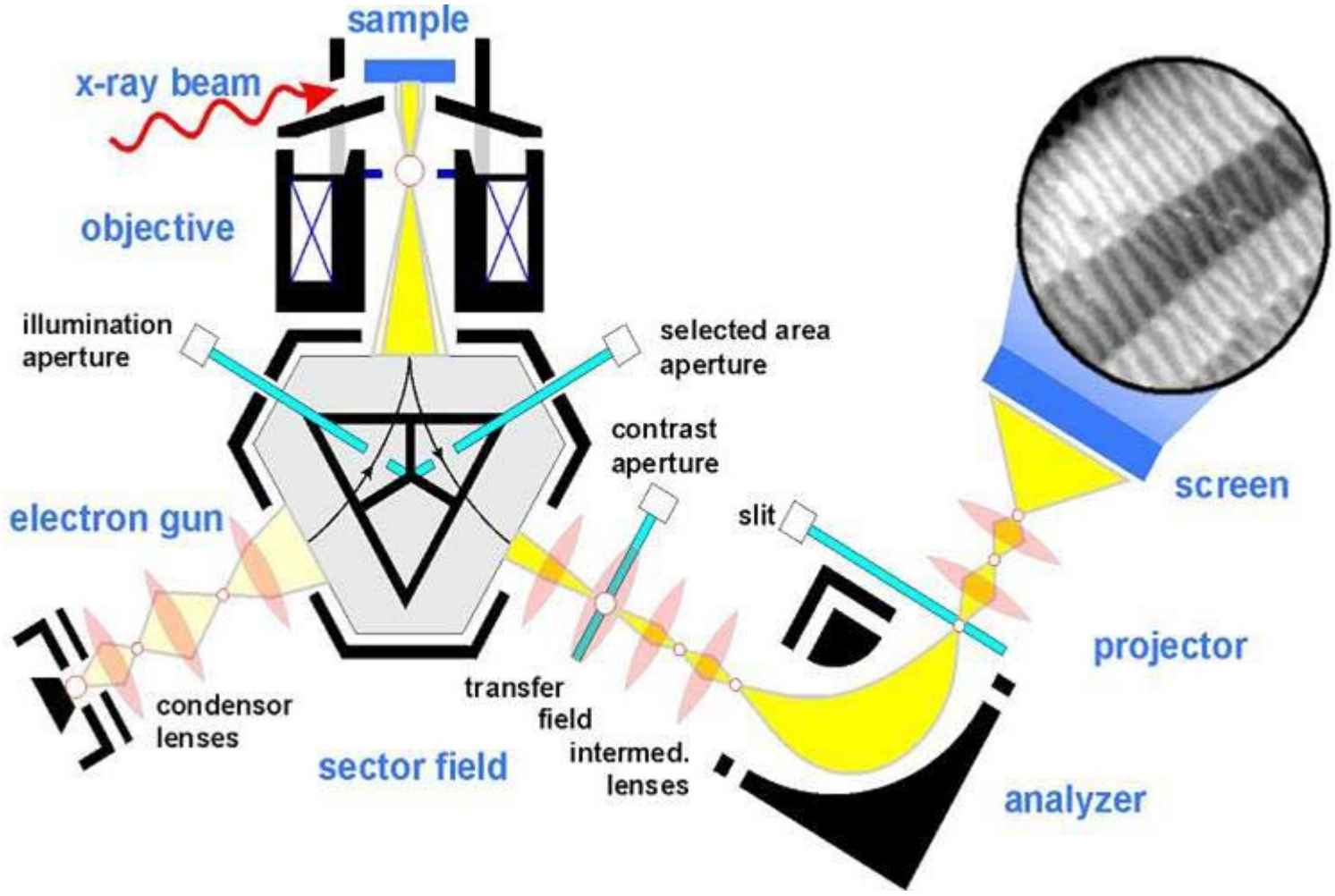

Imaging of the Dispersive Plane

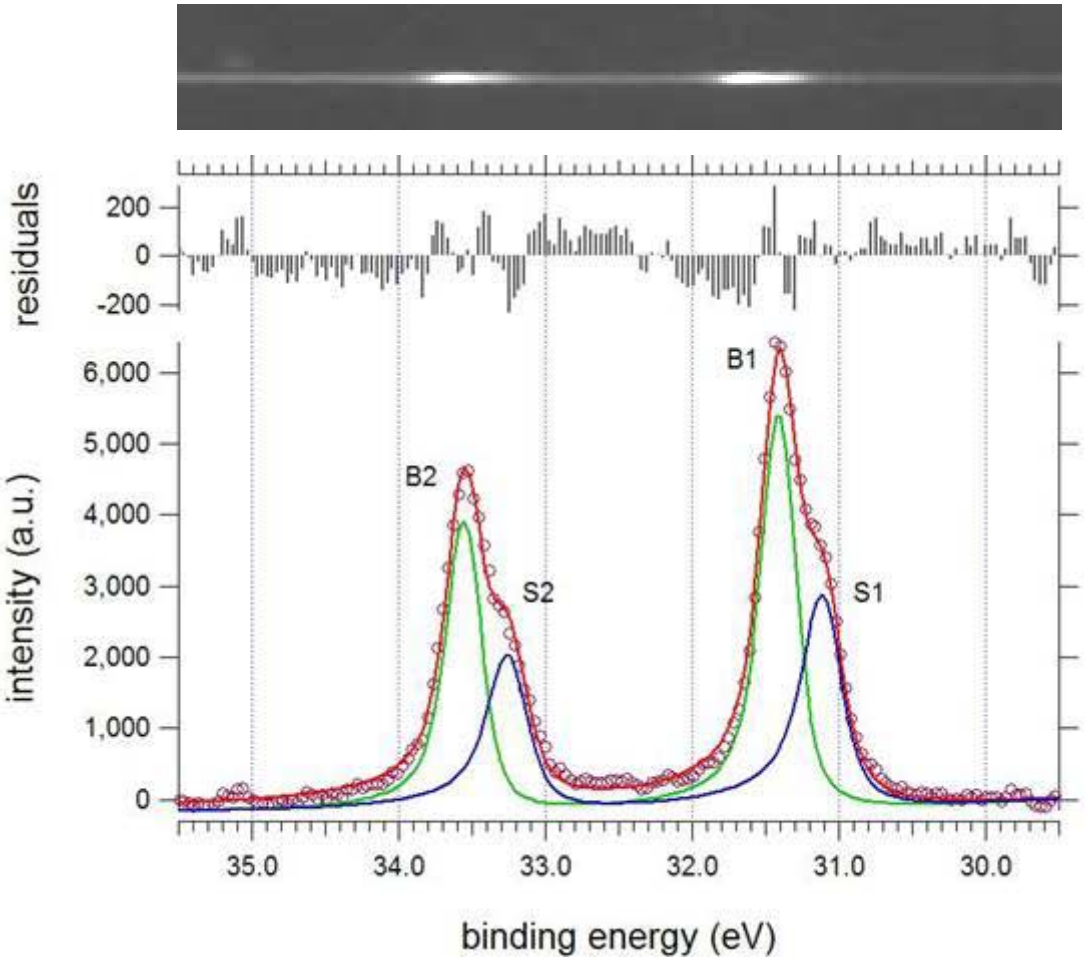

W{110} clean surface

W 4f core level

hv = 98 eV

Resolution 210 meV

parameter	Ref. (1)	Our fit
Gamma B (eV)	0.06	Fixed
Alpha B	0.035	Fixed
Gamma S (eV)	0.084	Fixed
Alpha S	0.063	Fixed
Gauss. Broad. (eV)	0.04	0.21
$W_{7/2}$-$W_{5/2}$ BE diff. (eV)	2.2 (2)	2.14
SCLS (eV)	0.321	0.304

(1) Riffe et al., PRL **63** (1989) 1976.
(2) Webelements

Lateral resolution

C 1s image (hv= 350 eV, KE = 62 eV)

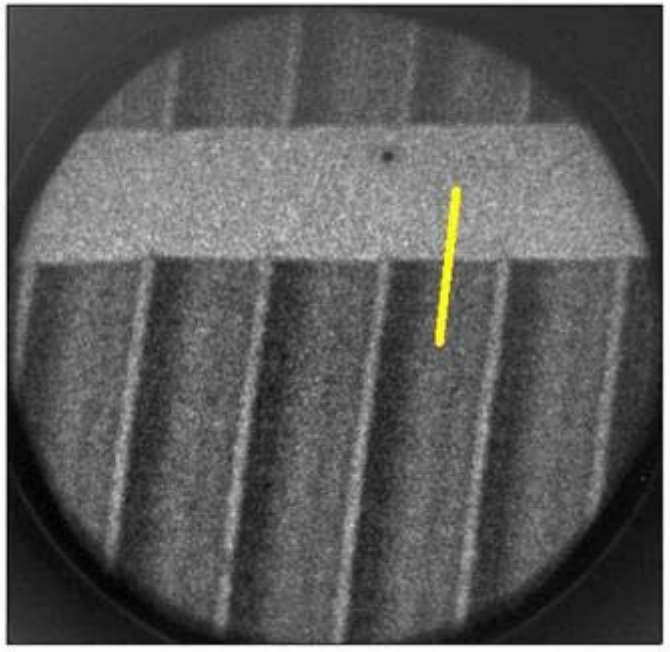

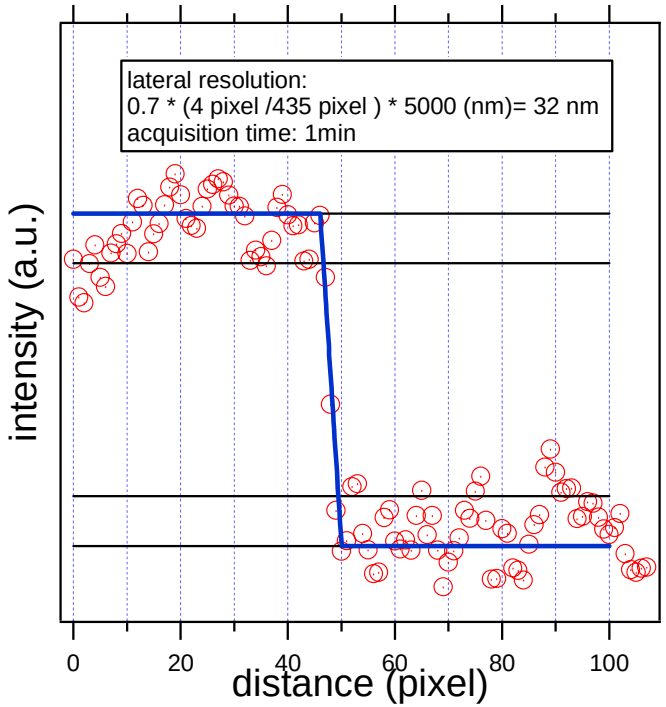

Lateral resolution: 32 nm

Example 1

VOLUME 86, NUMBER 22 PHYSICAL REVIEW LETTERS 28 MAY 2001

Spatial Variation of Au Coverage as the Driving Force for Nanoscopic Pattern Formation

Frank-J. Meyer zu Heringdorf,[1,*] Th. Schmidt,[2,†] S. Heun,[2] R. Hild,[1,‡] P. Zahl,[1]
B. Ressel,[2] E. Bauer,[3] and M. Horn-von Hoegen[1,‡]

[1]*Institut für Festkörperphysik, Universität Hannover, Appelstraße 2, 30167 Hannover, Germany*
[2]*ELETTRA, Sincrotrone Trieste, 34012 Basovizza TS, Italy*
[3]*Department of Physics and Astronomy, Arizona State University, Tempe, Arizona 85287*

(Received 9 October 2000)

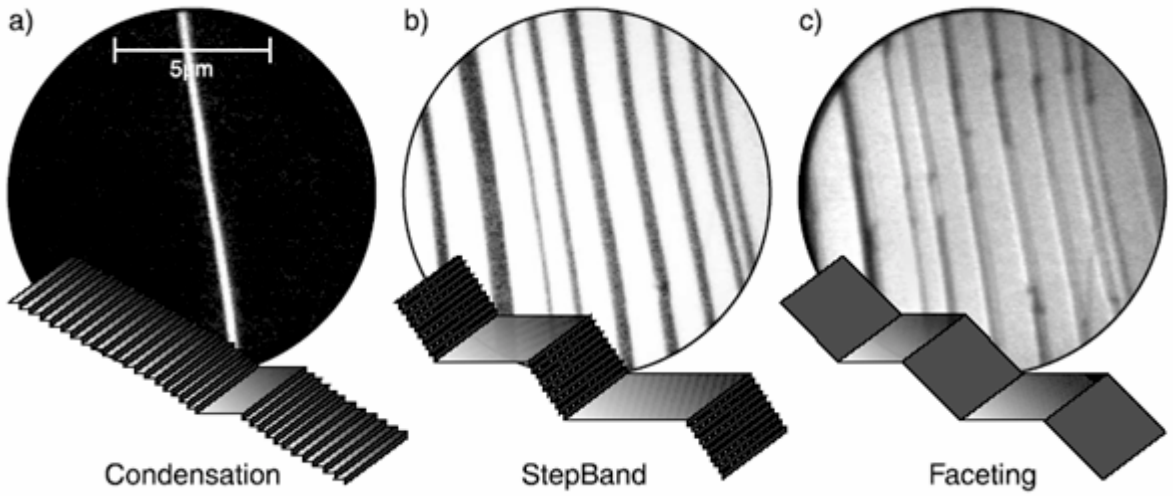

LEEM, XPEEM vs time

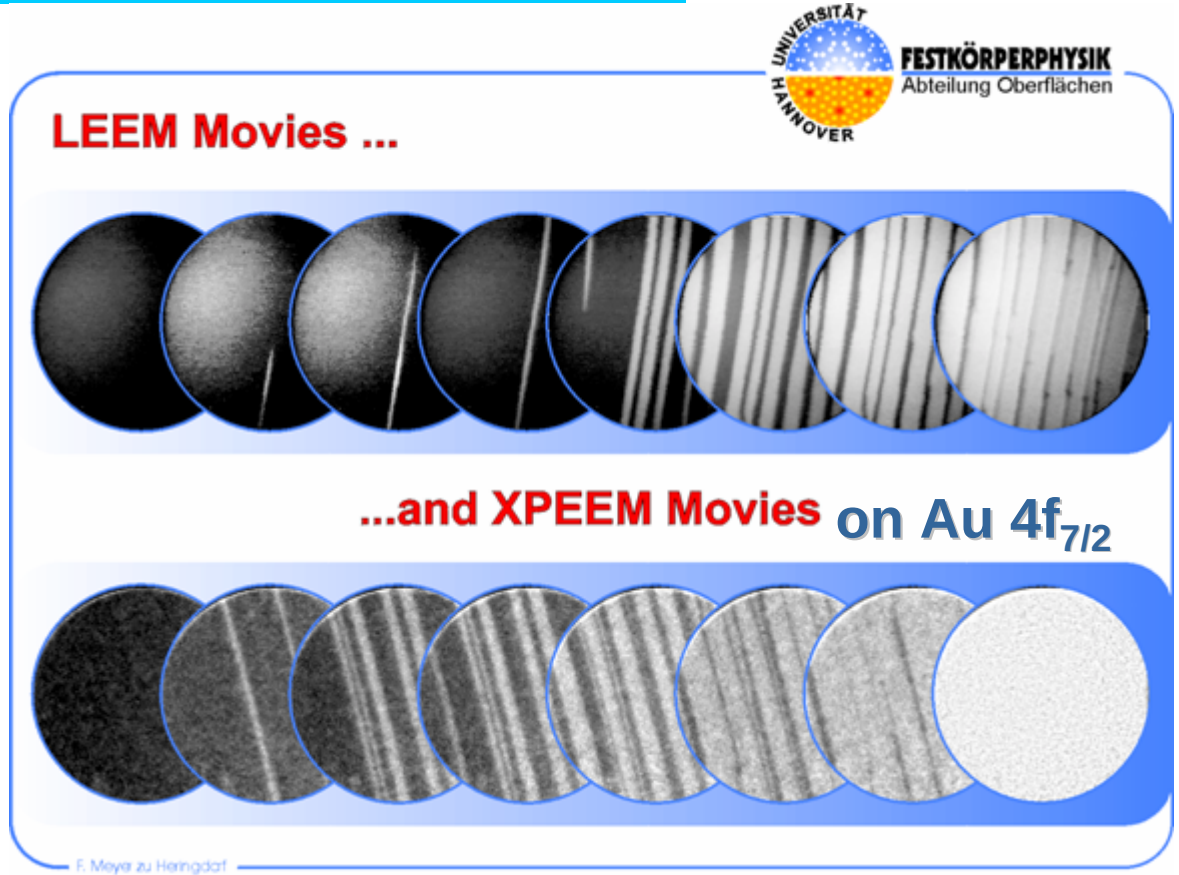

F.-J. Meyer zu Heringdorf, R. Hild, P. Zahl, Th. Schmidt, S. Heun, B. Ressel, E. Bauer, M. Horn-von Hoegen: Elettra News **36** (1999).

XPEEM imaging

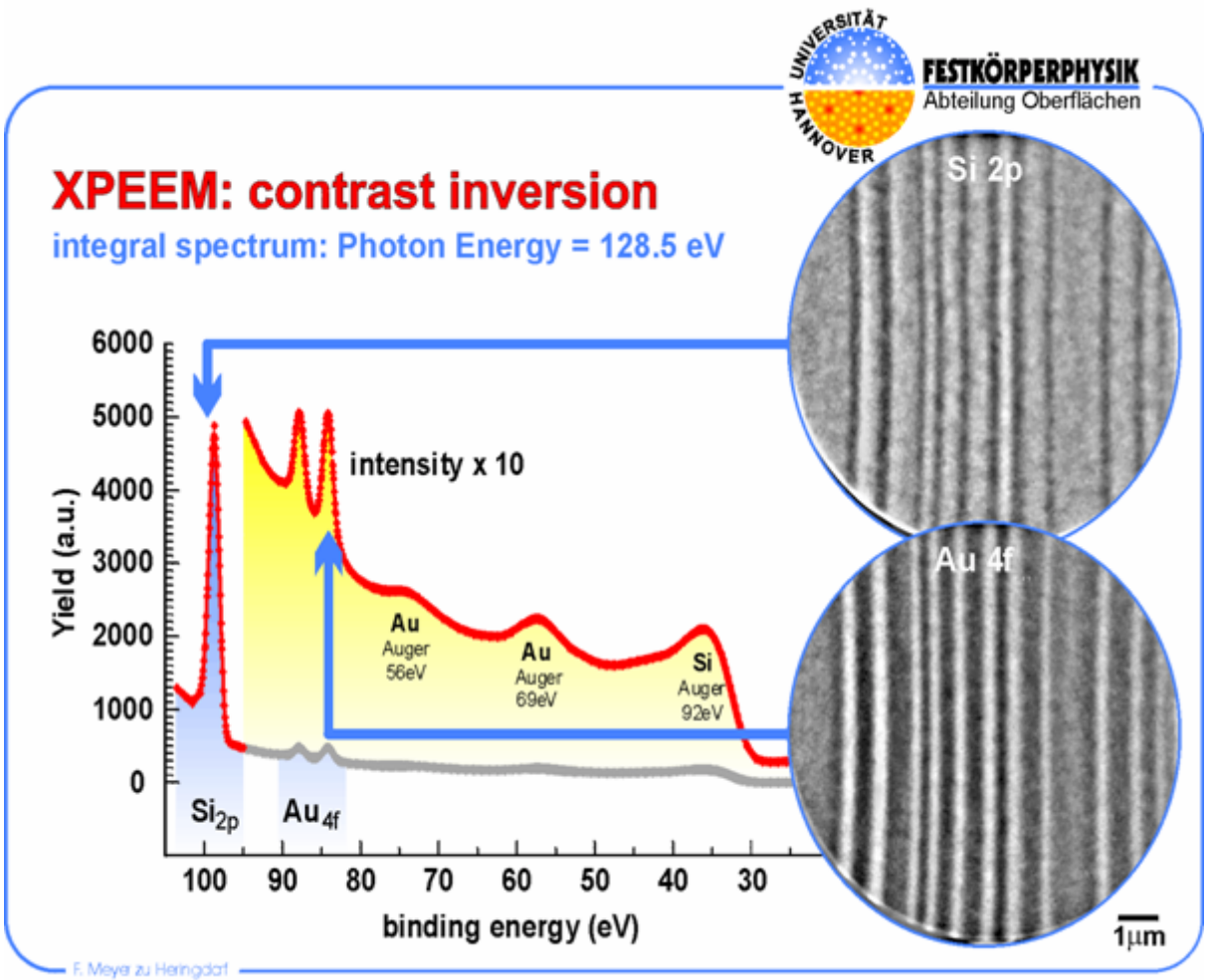

(001) terraces (LEEM)

F.-J. Meyer zu Heringdorf, Th. Schmidt, S. Heun, R. Hild, P. Zahl, B. Ressel, E. Bauer, M. Horn-von Hoegen: PRL **86** (2001) 5088.

Temporal evolution

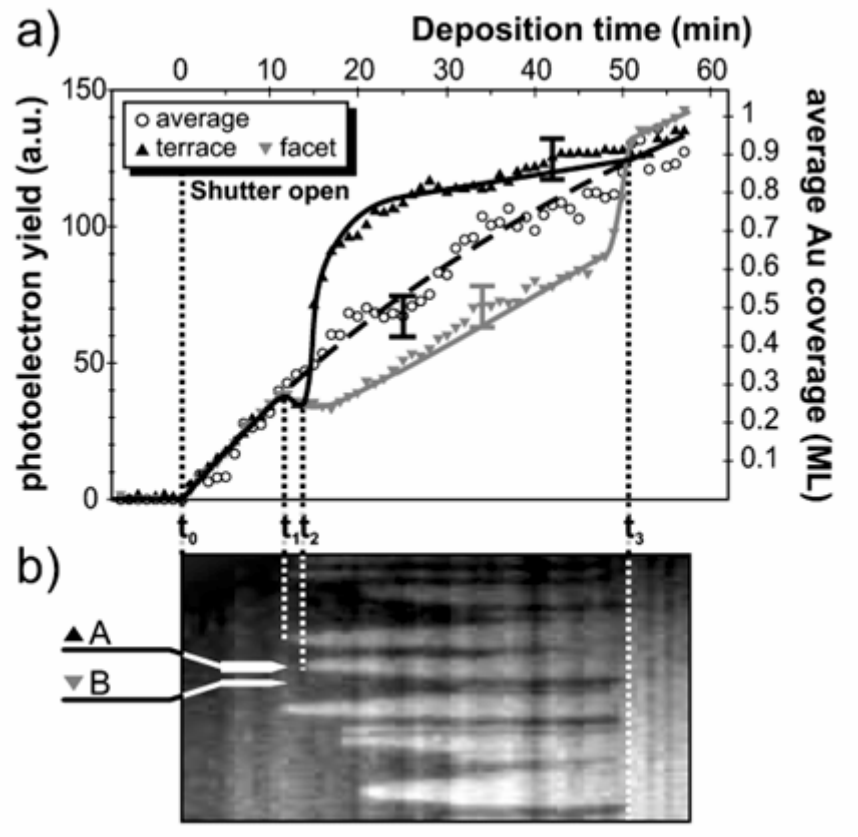

FIG. 3. Temporal evolution of the local Au coverage during faceting. (a) Au $4f_{7/2}$ photoelectron yield over deposition time. Absolute values of Au coverage on the right are calibrated by MEIS [17]. t_0: deposition starts, t_1: a first terrace is formed, t_2: a terrace is formed in the region of interest, t_3: the faceting is complete. (b) Slices from the XPEEM images analyzed in (a) were assembled to a time dependent grey scale representation. The arrows mark terraces analyzed in detail in (a).

Example 2

PHYSICAL REVIEW B, VOLUME 63, 125335

Core-level photoelectron spectroscopy from individual heteroepitaxial nanocrystals on GaAs(001)

S. Heun,[1,*] Y. Watanabe,[2] B. Ressel,[1] D. Bottomley,[2] Th. Schmidt,[1,†] and K. C. Prince[1]
[1]*Sincrotrone Trieste, Basovizza, 34012 Trieste, Italy*
[2]*NTT Basic Research Laboratories, Atsugi, Kanagawa 243-01, Japan*
(Received 26 September 2000; published 13 March 2001)

Core-level spectra of individual heteroepitaxial nanocrystals were measured with a spectroscopic photoemission and low-energy electron microscope that allows laterally resolved photoemission spectroscopy. The nanocrystals were obtained by depositing nominally 2 monolayers (ML) of InAs on a Se-terminated GaAs(001) surface. The Se-termination of GaAs results in the formation of a 2–3-ML-thick film of Ga_2Se_3 on top of bulk GaAs. During heteroepitaxy the InAs reacts with the Ga_2Se_3: A phase separation takes place on the anion sublattice, while an alloying takes place on the cation sublattice. During the initial stages of growth, a submonolayer-thick wetting layer of $In_xGa_{1-x}As$ is formed that is covered by $(In_yGa_{1-y})_2Se_3$. $(In_yGa_{1-y})_2Se_3$-covered InAs nanocrystals are formed on this surface.

DOI: 10.1103/PhysRevB.63.125335 PACS number(s): 79.60.Jv, 07.85.Qe, 85.35.Be

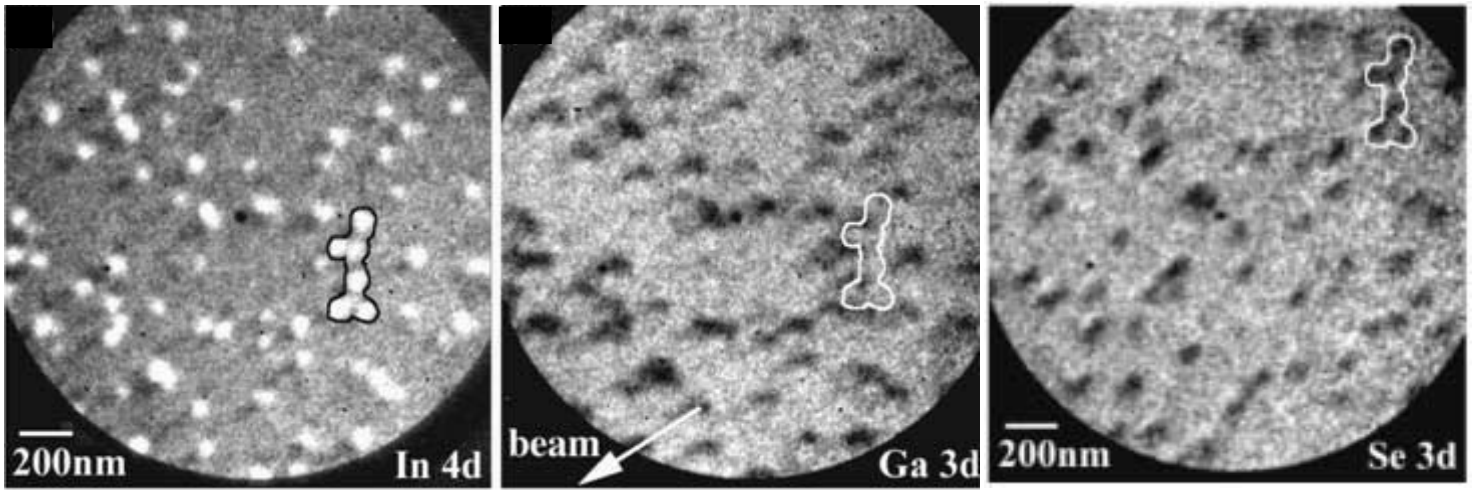

Laterally resolved XPS

Integral spectrum

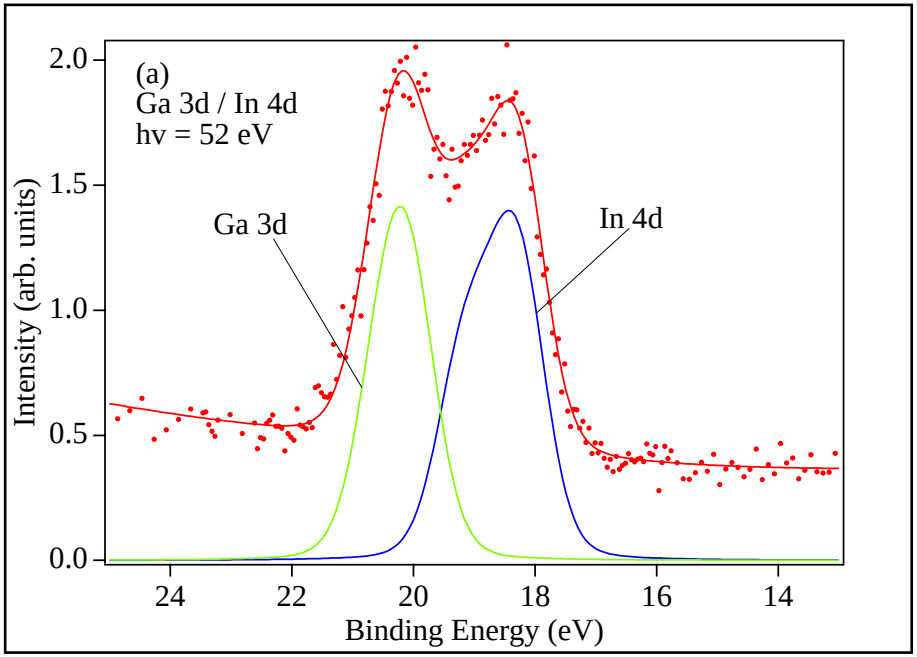

Laterally resolved spectra

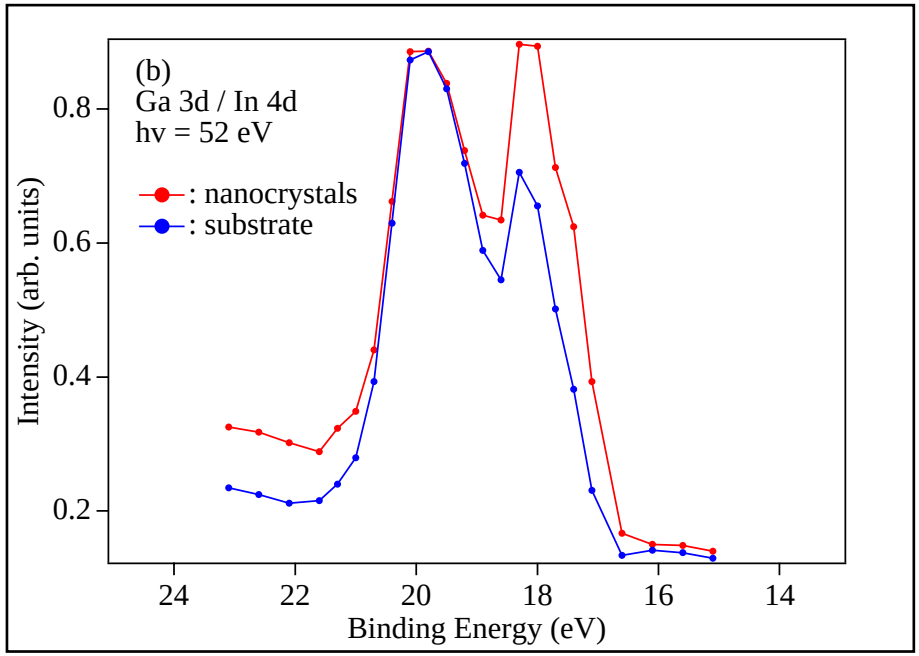

Indium on substrate ↑ SK growth mode
Gallium on nanocrystals

S. Heun, Y. Watanabe, B. Ressel, D. Bottomley, Th. Schmidt, and K. C. Prince, Phys. Rev. B **63** (2001) 125335.

Se 3d Core Level Spectra

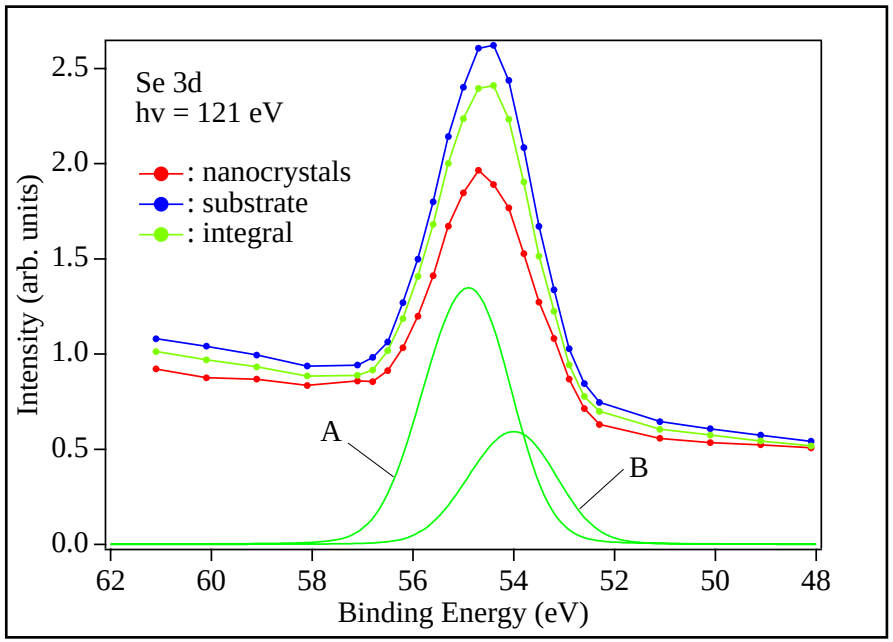

F. Maeda et al.: PRB **48** (1993) 4956.

- Ga_2Se_3: zincblende structure with ordered Ga vacancies.
- A: Se with no Ga vacancy as nearest neighbor
- B: Se with one Ga vacancy as nearest neighbor
- B species closer to the surface than A species
- clean Se/GaAs: A / B = 1.51

Here: intensity ratio A / B = 2.26

↑ less B species after deposition of InAs

↑ some material moved from surface to nanocrystals

From LEEM: volume of nanocrystals: 6 x 10^5 nm^3 per μm^2

2 ML InAs correspond to 6 x 10^5 nm^3 per μm^2

SK growth mode

↑ nanocrystal volume is greater than expected

↑ additional material from another source (Ga_2Se_3)

Example 3

re-organisation of a bimetallic surface under reaction conditions

A. Locatelli, S. Heun, M. Kiskinova
ELETTRA

motivations

Probing the morphology and composition of a mixed-metal surface under reaction conditions

- ***surface processes*** are governed by ***energetics*** with the interplay of ***diffusion*** of ad-species
  - segregation, surface alloying, reconstruction, clustering, lateral interactions ...
  - different reaction parameters may lead to the ***reorganisation of the surface*** [S. Günther et al, J. Electron Spectrosc. and Relat. Phenom. 114, 989 (2001)]
- Changes may occur on the ***atomic*** as well as on ***mesoscopic*** length scales

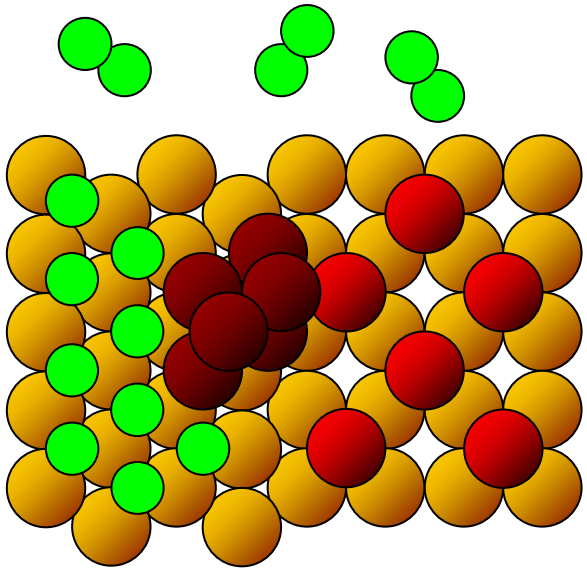

H_2+O_2 on Rh{110}

- **Bi-stability**
  - oxidised ↔ reduced
- **Meta-stability**
  - oxidised → reduced ┐
  - reduced → oxidised ┘

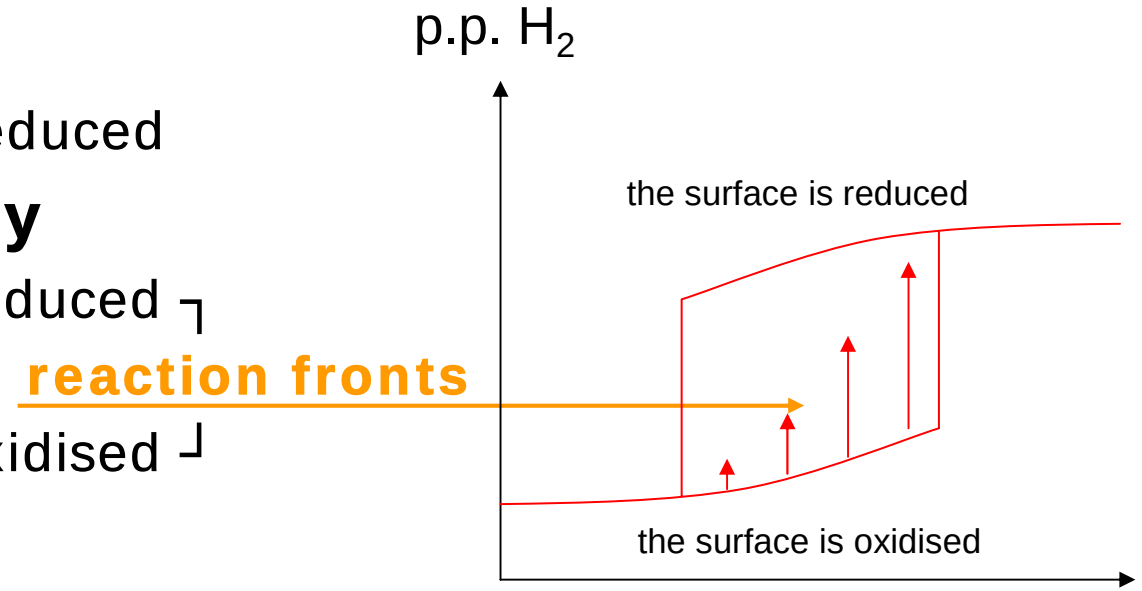

- **Elliptical shape of reaction fronts**
  - diffusion anisotropy
  - Site blocking effects

Mertens and Imbihl,
Chem. Phys. Lett. 242 (1995), 221-227;
Makeev and Imbihl,
J. Chem. Phys. 113 (2000), 1.

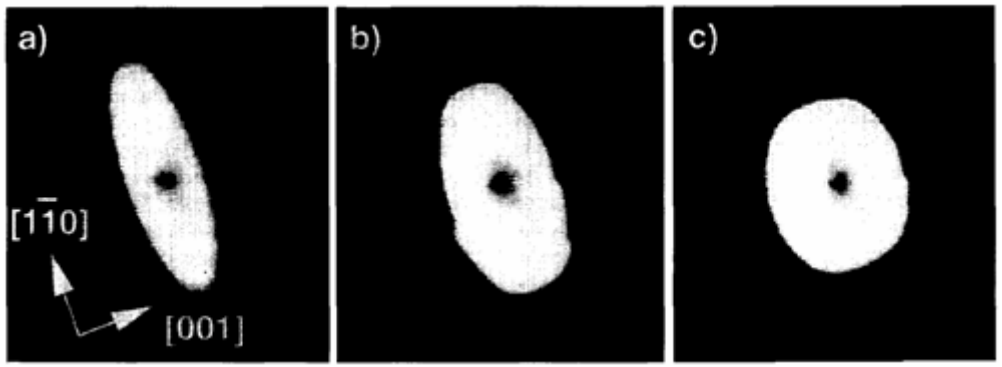

H_2+O_2 on Rh{110} - LEEM

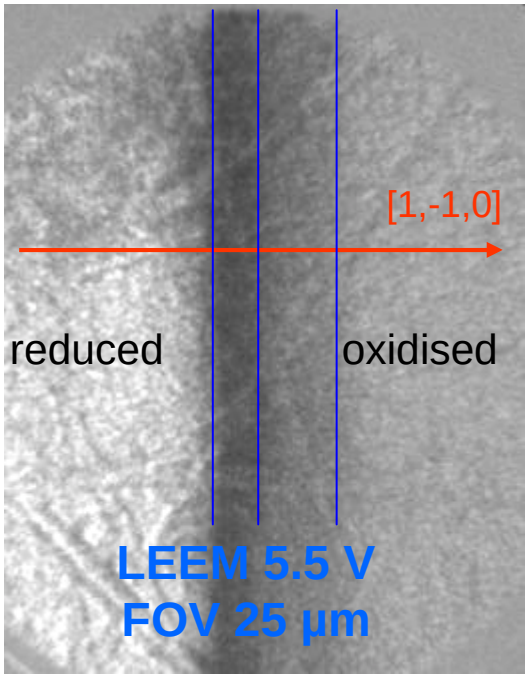

$p(O_2) = 3.2 \cdot 10^{-7}$ mbar
$p(H_2) = 8.0 \cdot 10^{-7}$ mbar
Sample temp. = 670 K

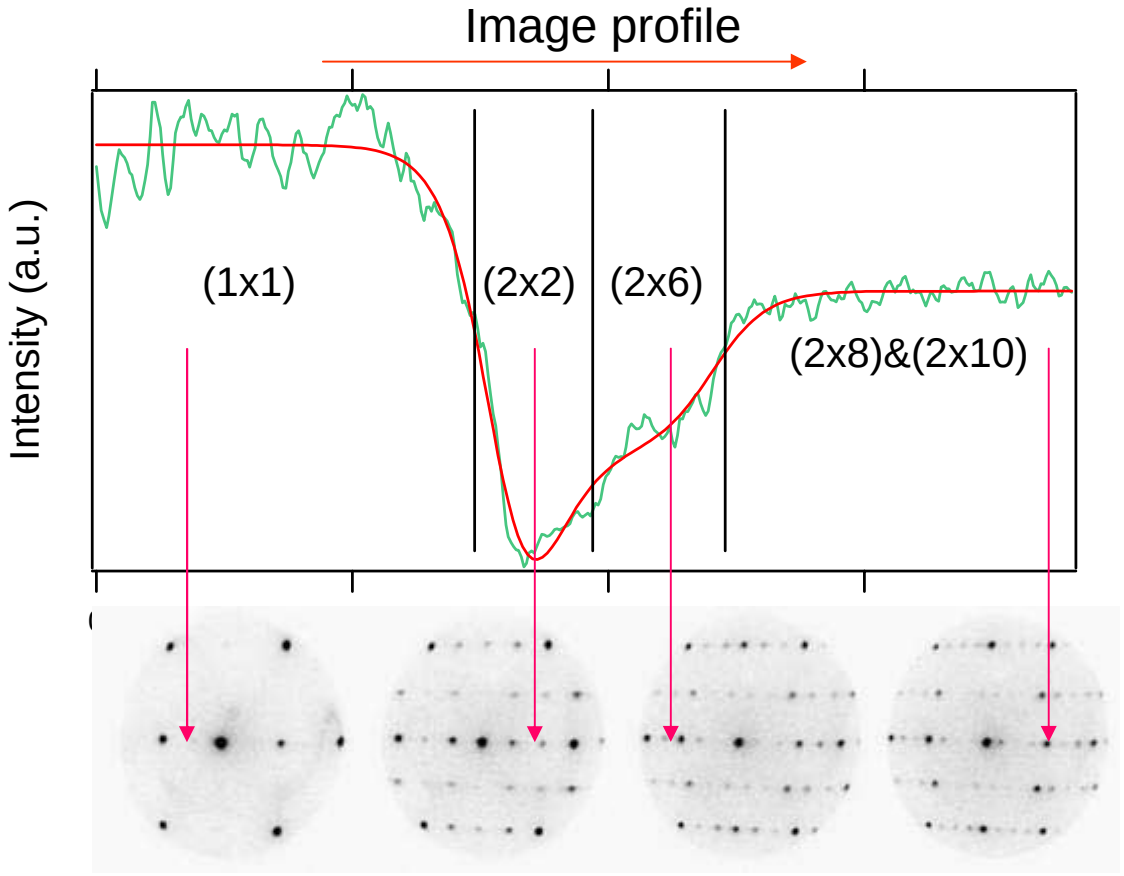

µLEED measurements

Wavefronts on Au-Rh{110}

LEEM field of view 20 µm

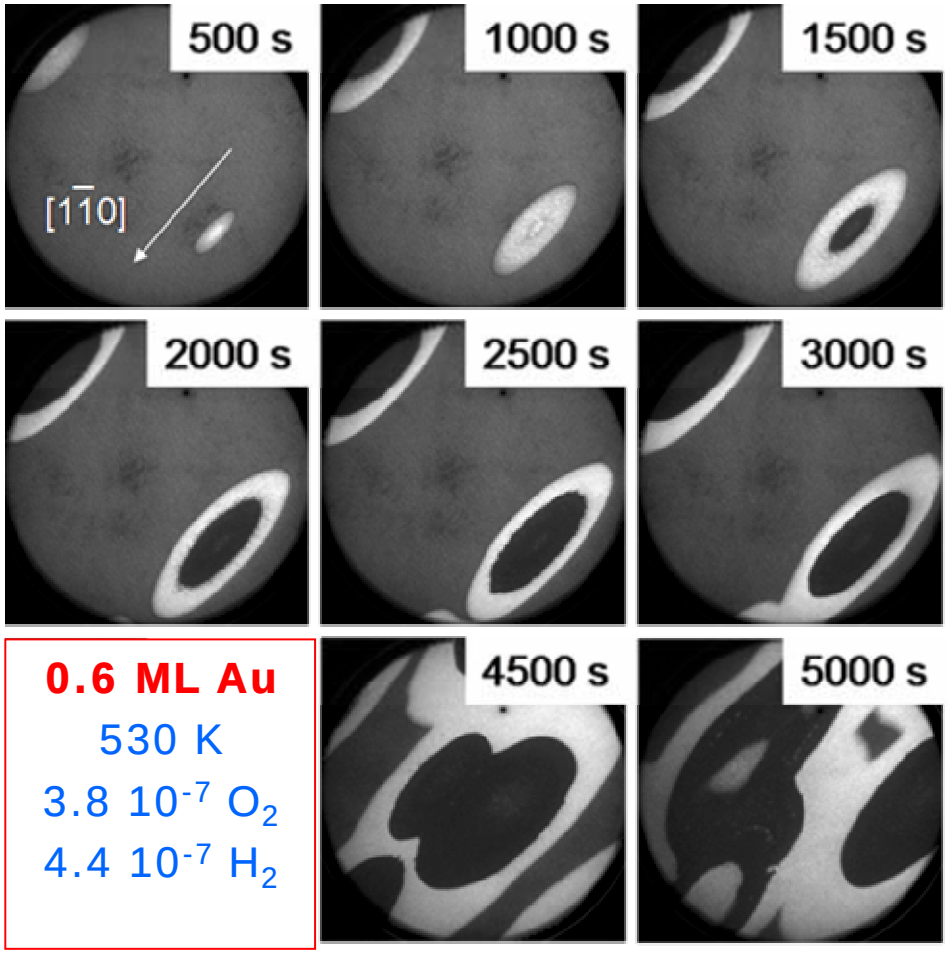

0.6 ML Au
530 K
3.8 10^{-7} O_2
4.4 10^{-7} H_2

XPEEM Au 4f

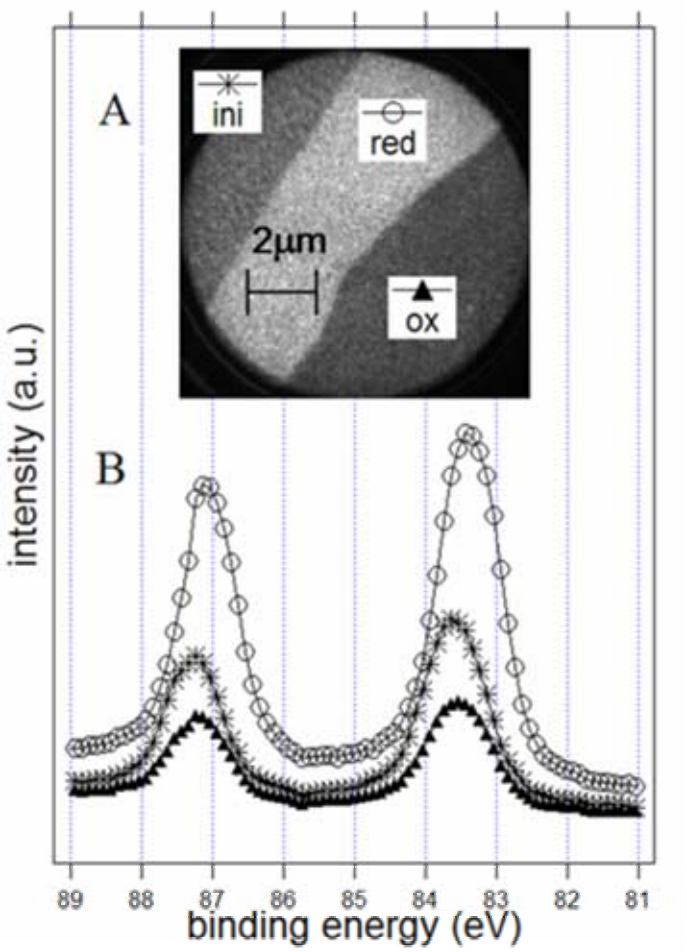

Stationary state

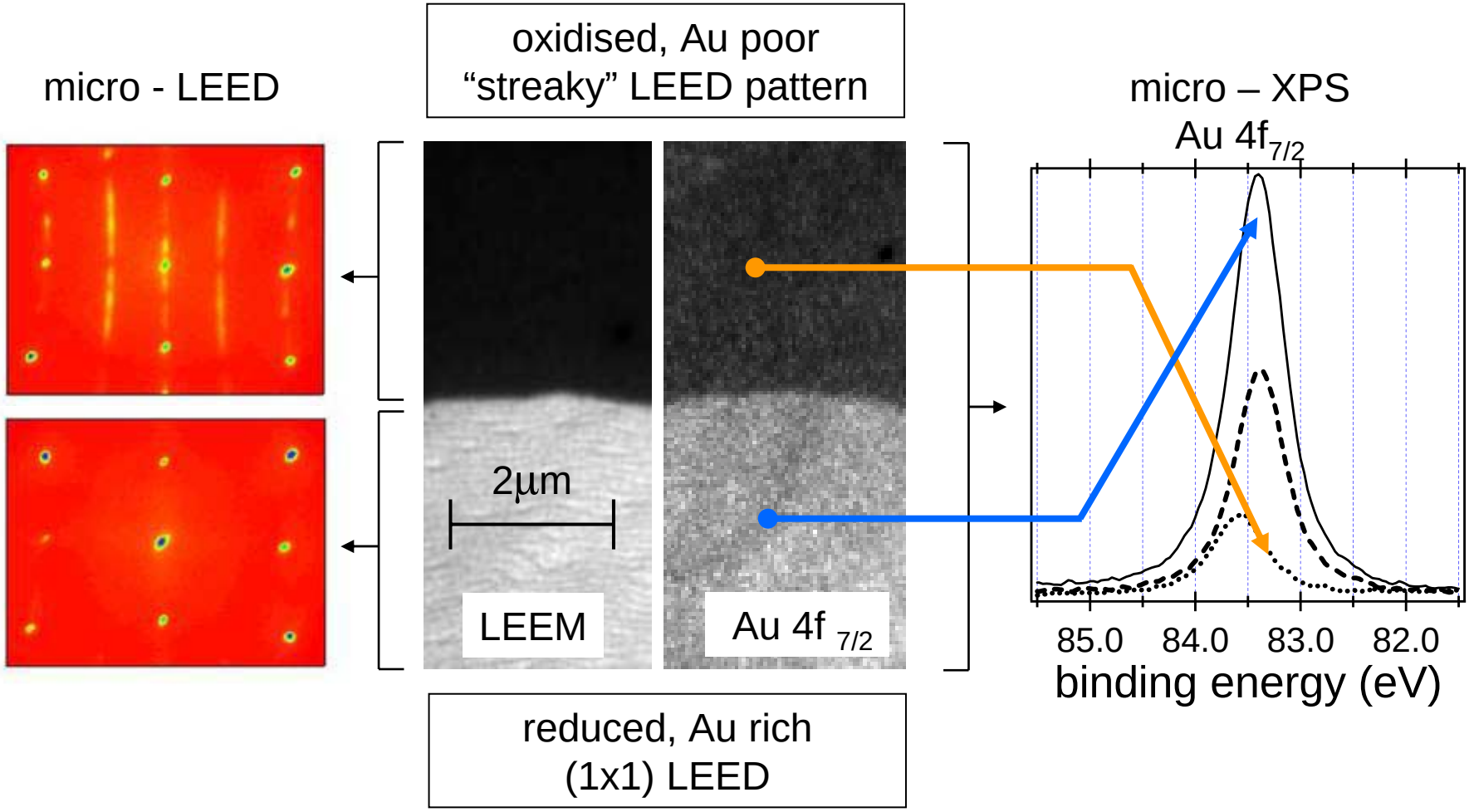

Pattern reactivity

- **Oxygen ambient: the pattern is preserved**

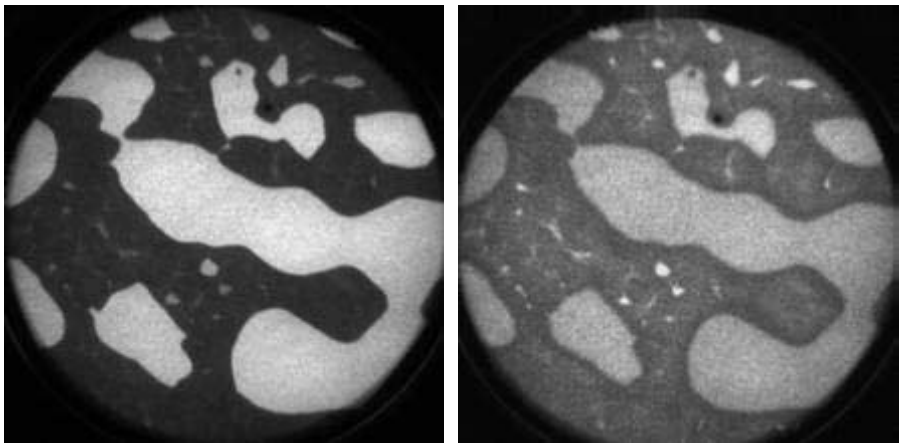

LEEM 7 V

field of view 20 µm

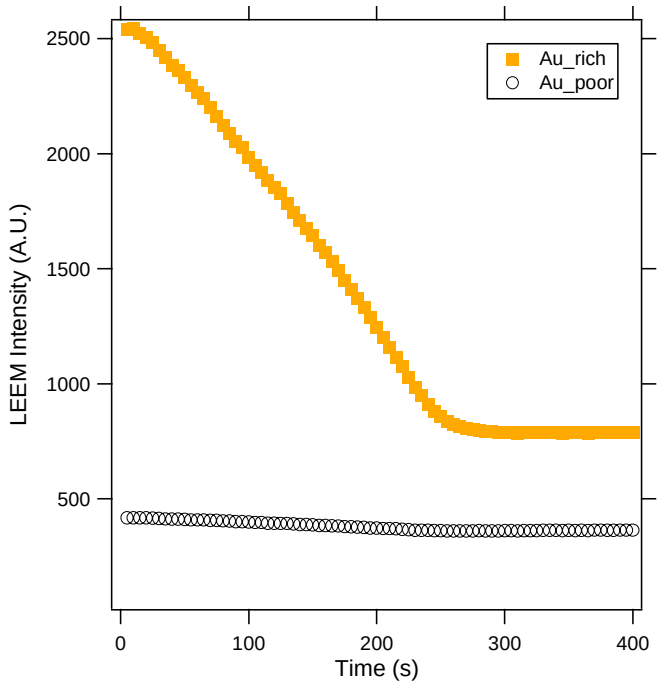

Pattern reactivity

- **Oxygen ambient: the pattern is preserved**
- **Hydrogen ambient: the pattern is destroyed**

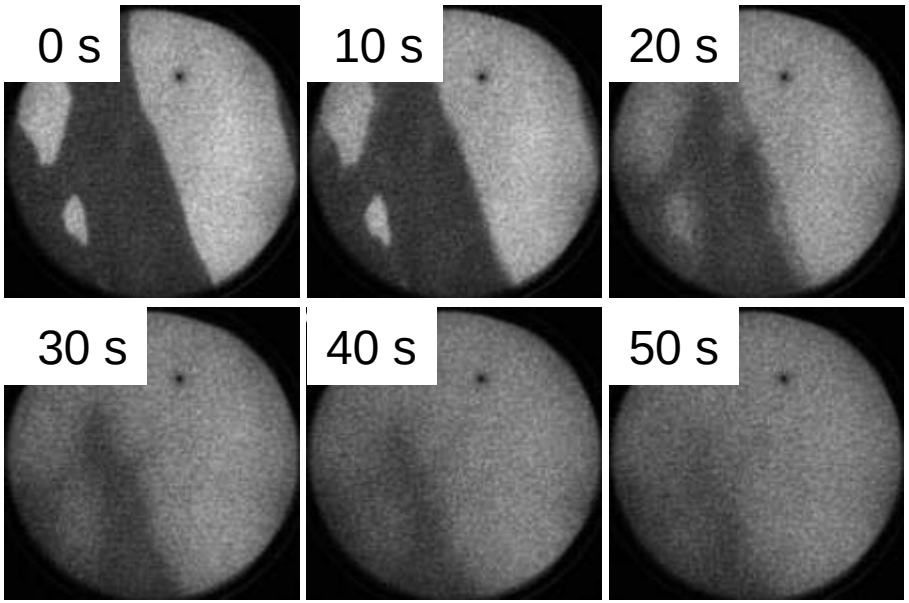

XPEEM Au 4f $_{7/2}$
field of view 10 μm

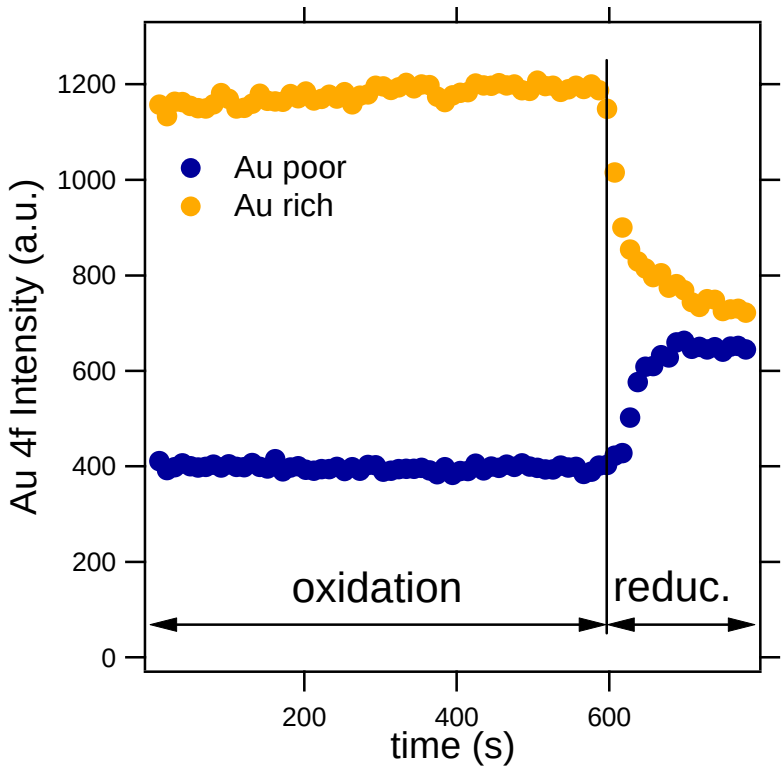

Au-Pd chemical mapping

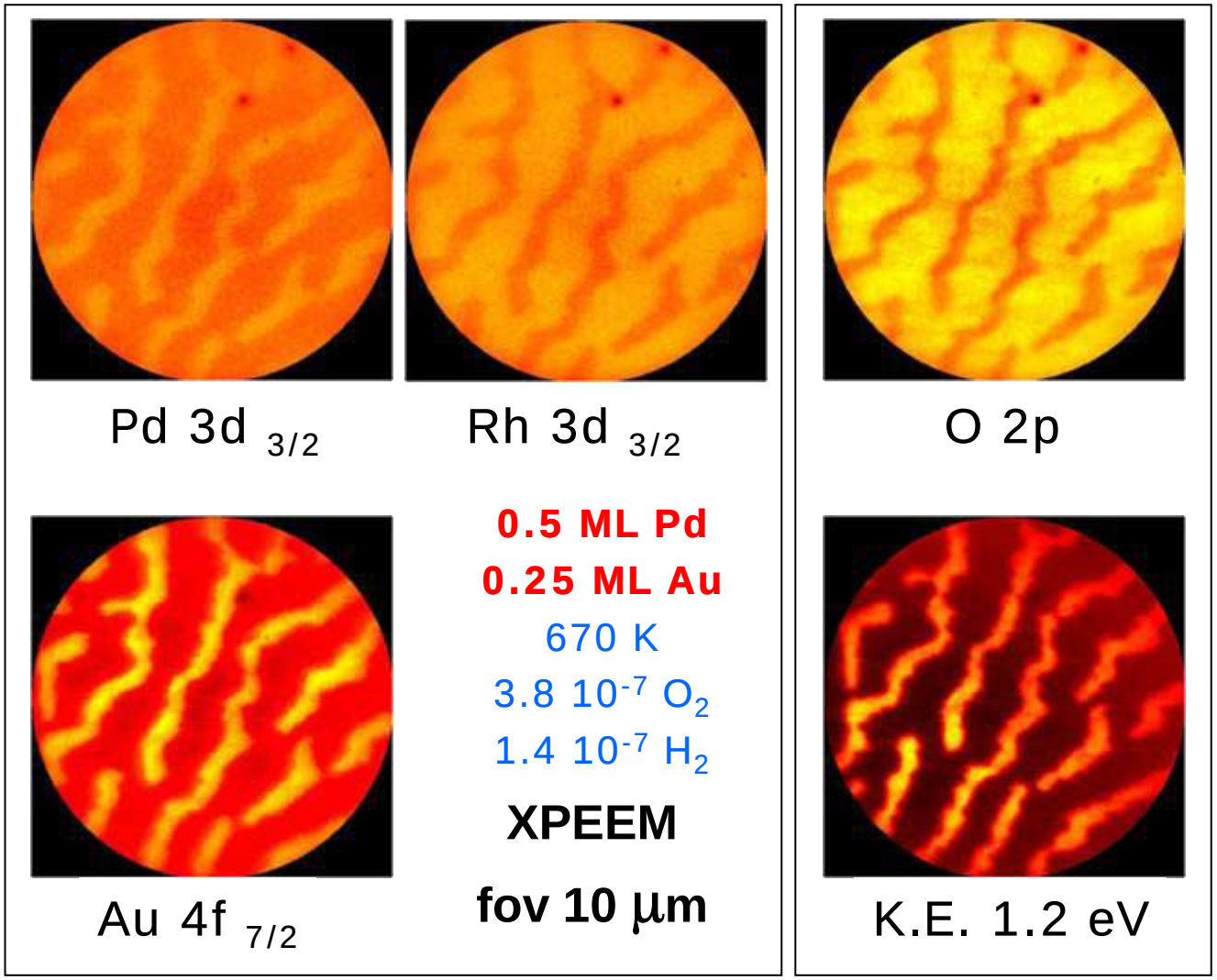

Summary

- The morphology and composition of a modified catalyst surface is strongly influenced by the **reaction conditions**

- The process is governed by the **interplay** between **diffusion** and **energetics** (i.e. the minimisation of the chemical potential

  key conditions for the redistribution to occur:
  - lateral attractive/repulsive interaction between adsorbates
  - Strong interaction Me-Rh

Image Processing

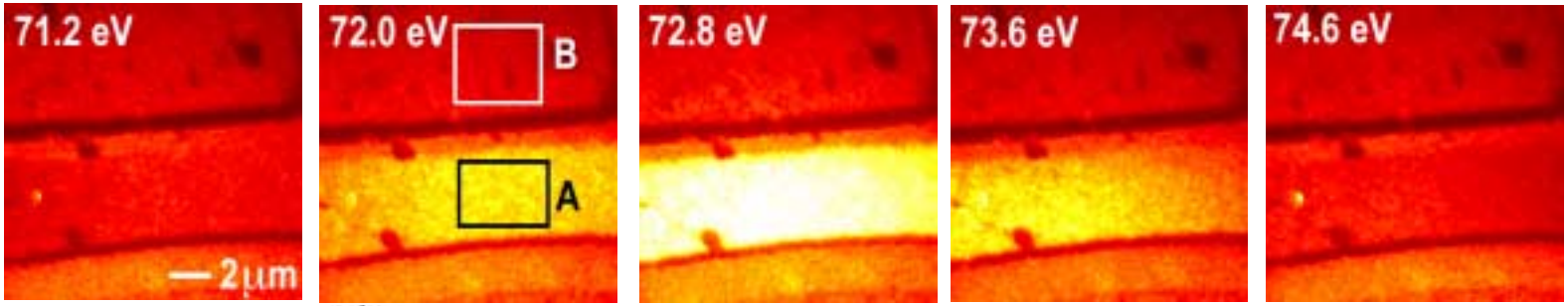

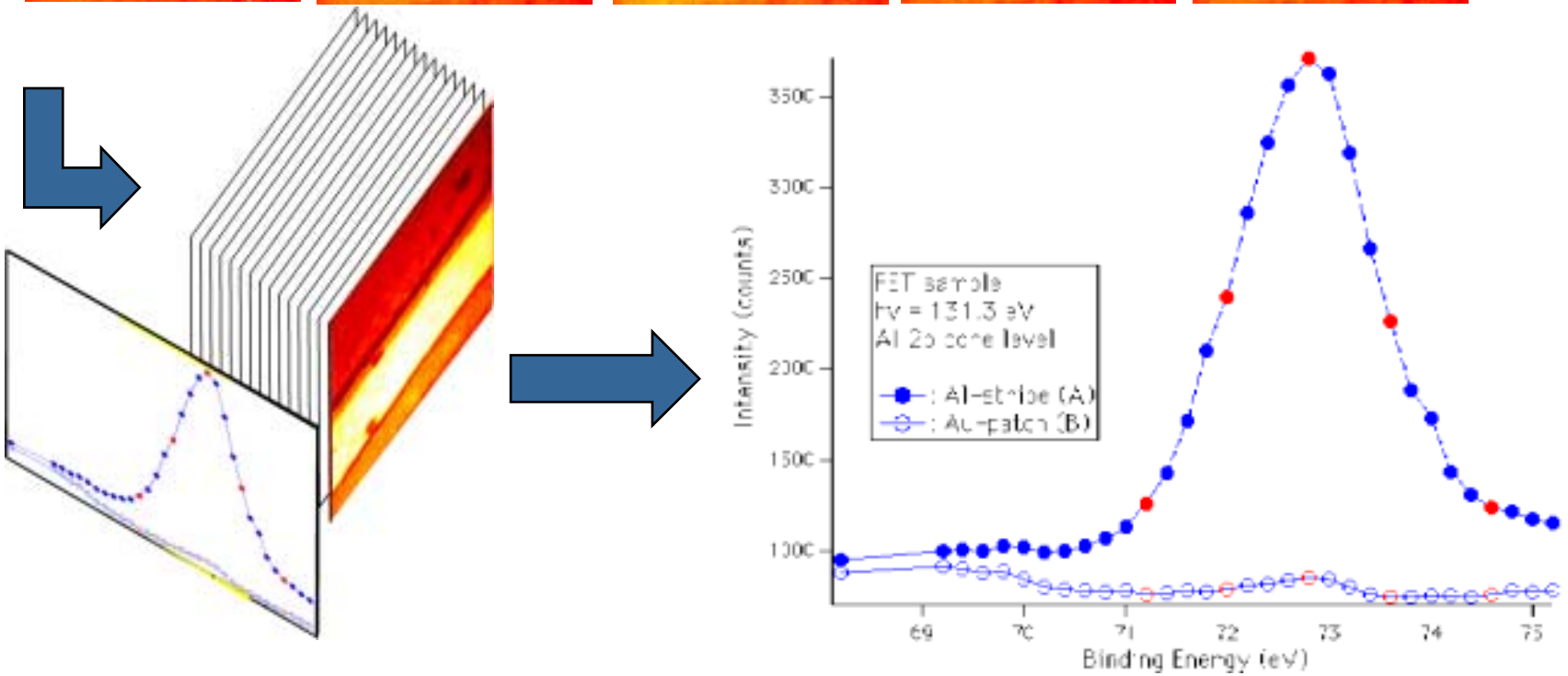

S. Heun, Th. Schmidt, B. Ressel, E. Bauer, and K. C. Prince, Synchrotron Radiation News Vol. 12, No. 5 (1999) 25.